Hindawi
Geofluids
Volume 2021, Article ID 1009766, 17 pages
https://doi.org/10.1155/2021/1009766

Research Article

Fluid Geochemistry within the North China Craton: Spatial Variation and Genesis

Lu Chang,[1,2] **Li Ying**,[1] **Chen Zhi**,[1] **Liu Zhaofei**,[1,3] **Zhao Yuanxin**,[1] **and Hu Le**[1]

[1]*CEA Key Laboratory of Earthquake Prediction, Institute of Earthquake Forecasting, Beijing, China*
[2]*Institute of Geophysics, China Earthquake Administration, Beijing, China*
[3]*State Key Laboratory of Geological Processes and Mineral Resources and School of Earth Science and Resources, China University of Geosciences, Beijing, China*

Correspondence should be addressed to Li Ying; liying@cea-ies.ac.cn

Received 26 May 2021; Revised 24 August 2021; Accepted 15 September 2021; Published 25 October 2021

Academic Editor: Andrew H. Manning

The North China Craton (NCC) is a typical representative of the ancient destruction craton. Numerous studies have shown that extensive destruction of the NCC occurred in the east, whereas the western part was only partially modified. The Bohai Bay Basin is in the center of the destruction area in the eastern NCC. Chemical analyses were conducted on 122 hot spring samples taken from the eastern NCC and the Ordos Basin. The δ^2H and δ^{18}O in water, δ^{13}C in CO_2, and ^{3}He/^{4}He and ^{4}He/^{20}Ne ratios in gases were analyzed in combination with chemical analyses of water in the central and eastern NCC. The results showed an obvious spatial variation in chemical and isotopic compositions of the geofluids in the NCC. The average temperature of spring water in the Trans-North China Block (TNCB) and the Bohai Bay Basin was 80.74°C, far exceeding that of the Ordos Basin of 38.43°C. The average δD in the Eastern Block (EB) and the TNCB were −79.22‰ and −84.13‰, respectively. The He isotope values in the eastern region (TNCB and EB) ranged from 0.01 to 2.52, and the rate of contribution of the mantle to He ranged from 0 to 31.38%. δ^{13}C ranged from −20.7 to −6.4‰ which indicated an organic origin. The chemical compositions of the gases in the EB showed that N_2 originated mainly from the atmosphere. The EB showed characteristics of a typical gas subduction zone, whereas the TNCB was found to have relatively small mantle sources. The reservoir temperatures in the Ordos Basin and the eastern NCC (EB and TNCB) calculated by the K-Mg temperature scale were 38.43°C and 80.74°C, respectively. This study demonstrated clear spatial variation in the chemical and isotopic compositions of the geofluids in the NCC, suggesting the presence of geofluids from the magmatic reservoir in the middle-lower crust and that active faults played an important role in the transport of mantle-derived components from the mantle upwards.

1. Introduction

A craton is characterized by a thick lithospheric mantle, cold geotherm, low density, and high viscosity, with these characteristics providing protection from destruction by later geological processes [1]. Cratons are an important geological unit on the surface of the Earth and cover ~50% of the area of the continental crust [2]. The North China Craton (NCC) is an ancient craton that has attracted much attention due to its lithosphere showing signs of severe disturbance or reactivation in some regions, resulting in significant losses or modifications of the mantle root (e.g., [3–9]).

The application of the *S*-wave receiver function showed that the eastern NCC has experienced extensive damage and that thinning of the lithosphere in the east and central parts of the NCC has exceeded that in the west by 60 to 100 km (Chen et al., 2009). Mineral inclusions in diamonds originating from the kimberlite in the provinces of Shandong and Liaoning, China, have indicated the existence of a 200 km thick lithosphere 470 Ma ago [10, 11]. In addition, the mantle-derived inclusions in Cenozoic basalts indicate a lithospheric thickness of 80–120 km [12]. Application of a geothermal evolution model found that the lithosphere experienced two thinning periods during the Cretaceous

and Paleogene. The lithosphere experienced thinning between the early Mesozoic to early Cretaceous, reducing in thickness from 150 km to 51 km, following which it thickened to ~80 km. The lithosphere experienced thinning again during the middle and late Paleogene, reducing in thickness to 48 km, consistent with the present thickness of the Bohai Bay fault depression. Subsequently, lithosphere thickening occurred once again, with the crust increasing in thickness to 78 km [13]. The results of a thermal simulation model indicated the presence of mantle heat flow of 24–44 $mW{\cdot}m^{-2}$ in the eastern NCC, which exceeded that of 21.2–24.5 $mW{\cdot}m^{-2}$ in the western NCC [14].

The study of geothermal fluids can increase the understanding of the geological significance of geothermal genesis, reservoir temperature, heating mechanism, circulation depth, and supply source [15–18] and can also act as a basis for exploring mantle-derived material and the shallow response resulting from the geodynamic process of plate subduction. The isotopic composition of gas is widely used to study deep structural changes and the transport mechanism in cratons (e.g., [19–24]).

Zhang et al. [25] analyzed the He and C isotope ratios of hot spring gases in the TNCB within the NCC. By analyzing the *P*-wave velocity and time-averaged fault slip rate, they concluded that mantle volatiles are generated in the upwelling asthenosphere, following which they rise through faults and fractures in which permeabilities are controlled by slip rates. In a study comparing the geochemical characteristics of helium and CO_2 in the cratonic and rift basins in China, Dai et al. [26] determined that gas samples collected from the cratonic basins have lower levels of CO_2 and R/Ra ratios than those from the rift basins. Gas samples in the rift basin have been shown to have a larger range of variation in $\delta^{13}C_{CO2}$, implying the presence of stronger tectonic activities. Xu et al. [27] determined that helium found in fluids collected from the crust in Liaodong (EB) is derived from the mantle and that active faults play an important role in transferring mantle-derived components to the surface in the nonvolcanic regions.

However, there have been limited detailed studies of mantle-derived components associated with the NCC [27–29]. Therefore, a study on the spatial differences in fluid chemistry and isotopic signatures of subduction zones and their genesis would be significant.

The present study collected samples of geothermal gases and water from the Ordos Basin, the TNCB, and the EB. The chemical compositions of water and gas samples were measured. In addition, the δD and $\delta^{18}O$ isotope compositions of water samples were determined. The gases collected from geothermal wells were analyzed for $^3He/^4He$ and $^4He/^{20}Ne$ ratios and $\delta^{13}C$ of CO_2. The present study was aimed at identifying the spatial variations in chemical and isotopic compositions of geothermal wells in the NCC and at analyzing the sources and genesis of these chemical characteristics. The thermal reservoir temperature and the contribution of mantle-derived helium were determined. The results of the present study confirmed the presence of mantle-derived components in the EB and TNCB gases due to magmatism and active faults.

2. Geological Settings

The NCC consists of two main crustal blocks, namely, the Western Block (WB) and the Eastern Block (EB). These two crustal blocks are stitched together by the Trans-North China Orogen (Figure 1(a)) [30]. The present study collected gas samples from the TNCB and the EB of the NCC (Figure 1), whereas geothermal water samples were collected from within the NCC (Figure 2).

The Bohai Bay Basin in the EB of the NCC is an important basin in China due to the presence of geothermal resources, oil, and gas. The basin lies adjacent to the Jiaoliao fault-uplift area in the east, the Liaohe Depression in the north, the Jiyang Depression in the south, and the Huanghua Depression in the west [32, 33]. The Bohai Bay Basin is a rift basin superposed by coal-bearing basins of the Meso-Cenozoic Carboniferous-Permian system lying on the basement of the Mesoproterozoic, upper Proterozoic, and Paleozoic cratons. The basin has experienced Indochina, Yanshan, and Himalayan movements and is characterized by active tectonic movements, numerous faults, and strong volcanic activities [34–36]. The study area shows a complex structure, the development of active faults, and frequent earthquakes. The main direction of stress in the study area is northeast-east, resulting in deep fault cuts [37]. Abundant low/medium-temperature pore-type geothermal resources and fractured bedrock occur in the region. Geothermal reservoirs are mainly found in the upper and lower tertiary sandstone reservoirs and particularly in Paleozoic and Proterozoic carbonate reservoirs [15, 38].

The basin-range tectonic zone of Shanxi Province falls in the North China orogenic belt. The BRPWB is characterized by northeast-east to southwest-west active normal faults with a dextral strike slip component due to its location on the north end of the S-shaped rift system [25]. The region has experienced many tectonic events and has a unique basin and mountain alternate topography as well as the geological background of the extensional fault along the mountains and within the basin. The counterclockwise movement of the EB and the WB in the NCC since the Paleogene has resulted in the formation of the basin-ridge structure [39] in the Trans-North China Orogen. Cenozoic basalts containing abundant mantle xenoliths were found in the outcrops of the Yangyuan and Datong subbasins in the EB [40, 41]. The age of geothermal water exposed at the junction of faults in the Yanhuai Basin was determined to be 30 ka, whereas the temperature of the reservoir was determined to be ~100°C. Mantle-derived helium was detected in the fluids [42]. These findings suggest that intensive magma activity and mantle-derived material recharge may have occurred in the region.

The Ordos Basin is in central-northern China and is associated with the inner-craton depression basin. The typical inland basin represents one of the most tectonically stable areas in China and has an area of over 250,000 m^2 [26]. The basin falls above and below the Archean granite and lower Proterozoic greenschist in the North China block, respectively. The southwest region of the basin contains Paleozoic-Cenozoic sedimentary rocks with a thickness of

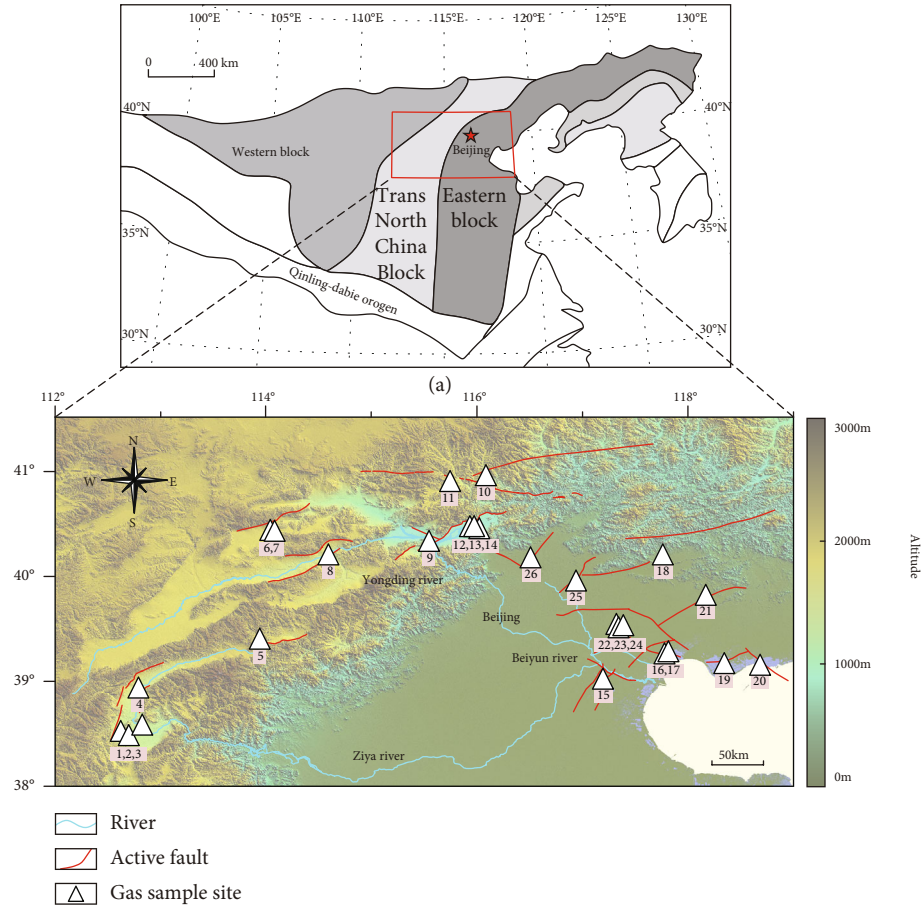

FIGURE 1: Distribution of gas samples collected from the North China Craton (NCC): (a) the subzones of the NCC, modified after Zhao et al. [31]; (b) the geological map of the Eastern Block (EB) and the Trans-North China Block (TNCB) showing faults and topography.

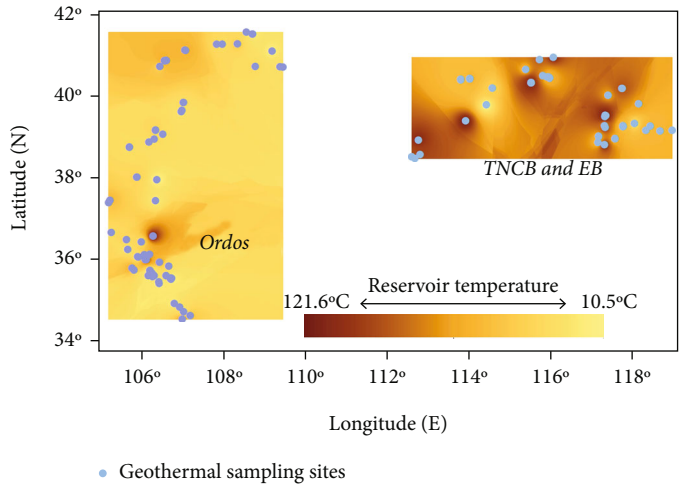

FIGURE 2: Interpolation diagram of a K-Mg ionic temperature scale in the North China Craton (NCC); numbers and names of sampling sites are listed in Tables 1 and 2. The interpolation method uses Inverse Distance Weighting (IDW).

>8 km [43]. Six secondary structures occur in the basin [26]: (1) the Yishan slope, (2) the Tianhuan depression, (3) the Yimeng uplift, (4) the Weibei uplift, (5) the Jin-West flexural fold zone, and (6) the fault fold zone along the western margin. The basin has undergone multiple tectonic movements with a stable internal structure. However, the overall uplift has played a key role [44]. The Fuping block collided with the Western Block at between 1.90 and 1.85 Ga and subducted westward to form the North China orogenic belt, accompanied by many magmatic events [45, 46]. The

sedimentary source is complex and experienced thickening in the basin after the Middle Proterozoic [47].

3. Methods

A total of 123 geothermal water samples were collected from July to August 2016, consisting of 46 samples from the TNCB and EB and 77 samples from the Ordos Basin. Figures 1 and 2 show the sampling locations. Samples were collected in HDPE bottles that had been sterilized by soaking in ultrapure water for 24 h and then dried using ultrasonic cleaning. Samples for the analysis of chemical compositions and isotopes (H and O) were collected in 250 mL and 2 mL HDPE bottles, respectively. All samples were filtered on-site three times through a 0.45 μm membrane filter. Prior to sampling, the sample bottle was rinsed three times using water from the sample source. Once the sample was collected, the sample bottle was sealed with parafilm. Samples for the analysis of major cations were acidified with ultrapurified HNO_3 (1 mol L^{-1}) to adjust pH to below 2. Filtered unacidified samples were used for anion analysis. Tables 1 and 2 show the results of water chemistry and isotopic analysis, respectively.

The water temperatures of springs were measured using a thermometer with an accuracy of 0.1°C. Water chemistry analyses were performed in the Key Laboratory of Earthquake Prediction, Institute of Earthquake Science, China Earthquake Administration, using a DionexICS-900 ion chromatograph with an ion detection limit 0.1 mg L^{-1}. Calibration for the analysis was achieved using standard samples from the National Institute of Metrology, China. A mixed solution of $NaHCO_3$ and Na_2CO_3 was used as the anion eluent, whereas a methane sulfonic acid solution was used as the cationic eluent. The titration method with an error less than 5% was used for analyzing CO_3^{2-} and HCO_3^-, phenolphthalein and methyl orange were used as indicators, and the test error of the concentration of HCl was 0.08 mol L^{-1}. Oxygen and hydrogen isotope analyses were performed in the Water Isotope and Water-Rock Interaction Laboratory at the Institute of Geology and Geophysics, Chinese Academy of Sciences, using a laser absorption water isotope spectrometer analyzer (L1102-I, Picarro) which used wavelength scanning optical cavity ring-down spectroscopy (WS-CRDS) technology. Analysis of $\delta^{18}O$ and δD used the Vienna Standard Mean Ocean Water (V-SMOW) as the standard. The analytical precision of $\delta^{18}O$ and δD measurements was ±0.1‰ and ±0.5‰, respectively [37].

The quality of the constant elements of hot spring and geothermal water was assessed using the ib value [48], with the range of results within ±10%:

$$\mathrm{ib}[\%] = \frac{\sum \mathrm{cations} - \sum \mathrm{anions}}{0.5 \times (\sum \mathrm{cations} + \sum \mathrm{anions})} \times 100. \quad (1)$$

A total of 26 gas samples were collected from TNCB and EB. The gas samples were collected using the water displacement method.

The present study used 500 mL AR glass containers, with the glass of the soda lime type containing a high portion of alkali and alkaline earth oxides with a very low permeability for helium [49]. The glass containers were initially immersed in corresponding geothermal water. The bottles were filled with spring water, following which funnels allowed displacement of water with gas. After the gas reached two-thirds of the volume of the bottle, each bottle was forcefully sealed using a solid trapezoidal rubber plug and adhesive plaster [50]. Samples were analyzed within 14 days after collection to avoid the leakage of volatiles.

The chemical compositions of the gas sample were analyzed using a Finnigan MAT-271 mass spectrometer with precision of ±0.1% at the Key Laboratory of Petroleum Resources Research, Institute of Geology and Geophysics, Chinese Academy of Sciences. The helium and neon isotopes of the gases were detected using a MM5400 mass spectrometer at the Institute of Geology and Geophysics, Chinese Academy of Sciences. The carbon isotope was measured with the MAT-253 gas isotope mass spectrometer of the Beijing Research Institute of Uranium Geology, with a precision of ±0.1‰ [51].

Rc/Ra is the air-corrected $^3He/^4He$ ratio calculated using

$$\frac{\mathrm{Rc}}{\mathrm{Ra}} = \frac{[(\mathrm{R/Ra} \times X) - 1]}{X - 1}, \quad (2)$$

$$X = \frac{\left(^4\mathrm{He}/^{20}\mathrm{Ne}\right)_{\mathrm{measured}}}{\left(^4\mathrm{He}/^{20}\mathrm{Ne}\right)_{\mathrm{air}}} \times \frac{\beta_{\mathrm{Ne}}}{\beta_{\mathrm{He}}}. \quad (3)$$

β is the Bunsen solubility coefficient, which represents the volume of gas absorbed per volume of water at the measured temperature when the partial pressure of the gas is 1 atm [52], assuming a recharge temperature of 15°C. $\beta_{Ne}/\beta_{He} = 1.21$ at 15°C. He_M is the mantle helium contribution of the total helium contents using

$$\frac{\mathrm{Rc}}{\mathrm{Ra}} = \left(\frac{\mathrm{R}}{\mathrm{Ra}}\right)\mathrm{crust} \times (1 - \mathrm{He_M}) + \left(\frac{\mathrm{R}}{\mathrm{Ra}}\right)\mathrm{mantle} \times \mathrm{He_M}. \quad (4)$$

According to [53], (R/Ra)mantle = 8; according to [54], (R/Ra)crust = 0.02.

4. Results

The average temperatures of spring water in the Bohai Bay Basin, the TNCB, and the Ordos Basin were 55.0°C, 46.1°C, and 19.4°C, respectively. The geothermal water in the Ordos Basin comprised natural hot springs or artesian wells, and there are no data for the depth of wells. The gas components in the geothermal water were mainly N_2, O_2, Ar, CH_4, and CO_2. N_2 was the predominant gas component in all samples. The concentrations of heavier hydrocarbons, H_2S, SO_2, and H_2 fell below their respective detection limits. The ranges of concentration of N_2 and O_2 of nitrogen-rich hot springs were 69.42–98.52% and 0.07–18.57%, respectively. The concentration of Ar ranged between 0.92 and 1.47%, similar to that of air. The concentration of CO_2 ranged between 0.01 and 7.91%, which is some several

Table 1: Sampling locations, water temperatures, isotopes (H and O), and reservoir temperatures in the Eastern block and the Trans-North China Block of the North China Craton.

Well no.	Longitude (°E)	Latitude (°N)	Na^+ (mg/L)	K^+ (mg/L)	Mg^{2+} (mg/L)	Ca^{2+} (mg/L)	HCO_3^- (mg/L)	Cl^- (mg/L)	SO_4^{2-} (mg/L)	IB (%)	$T_{K\text{-}Mg}$ (°C)	T (°C)	$\delta^{18}O$ (‰)	δD (‰)	Well depth (m)
Guanghegu	117.17	38.89	674.1	6.8	7.4	40.1	261.3	600.0	773.5	-3.9	60.9	51.0	-9.0	-71.7	—
Liyuantou	117.19	39.03	642.6	5.7	2.8	26.9	303.6	532.7	670.9	-3.7	67.8	56.7	-9.2	-72.3	—
Wanjia	117.33	38.83	585.7	57.0	7.1	33.1	449.6	663.8	334.0	-3.5	115.8	62.9	-8.7	-70.8	490
Longda	117.59	38.97	554.1	5.0	2.2	13.0	564.9	434.5	256.9	-2.2	67.6	50.5	-8.9	-71.2	1800
Quanshuiwan	117.33	39.29	306.1	2.3	0.9	5.8	626.4	119.8	15.1	-1.0	60.3	51.6	-9.2	-72.5	1500
Yongchuan	117.35	39.25	406.1	77.1	11.4	33.9	399.7	390.1	310.8	-2.1	117.7	81.2	-8.8	-71.5	3000
Xinli	117.79	39.28	144.5	1.1	0.2	6.1	314.9	21.7	33.6	-1.8	57.7	49.3	-9.6	-72.2	1000
Xiawucun	117.78	39.27	149.4	1.2	0.3	5.7	330.5	23.4	32.5	0.0	58.0	53.0	-9.5	-72.0	—
Luqiancun	117.78	39.29	110.6	1.3	0.1	5.0	284.4	13.6	10.4	-1.1	71.6	44.9	-9.6	-71.8	—
Zunhua 1	117.76	40.21	211.4	6.4	0.5	22.6	126.8	32.6	364.0	-1.1	91.0	46.1	-10.3	-74.0	—
Zunhua 2	117.76	40.21	198.7	6.2	0.3	17.8	99.9	33.4	333.0	-0.5	97.9	41.4	-10.3	-73.7	—
Xiyuan	118.06	39.34	179.2	0.9	0.8	11.0	292.1	31.5	130.1	0.0	41.6	40.2	-9.6	-71.2	—
Jidong 1	118.45	39.28	275.5	3.9	1.4	24.5	215.2	75.9	396.6	-1.1	67.0	46.4	-9.4	-71.5	—
Jidong 2	118.34	39.18	609.7	6.8	3.8	66.8	222.9	560.6	739.6	-3.9	68.3	50.5	-8.3	-70.8	1500
Caofeidian	118.68	39.16	321.7	2.2	0.5	17.2	522.3	122.0	143.6	-2.3	66.3	50.4	-9.2	-70.7	—
Xiangyunwan	118.98	39.18	630.3	4.1	1.3	4.0	1437.3	216.1	0.0	-1.9	69.3	56.3	-9.0	-70.8	1800
Changsheng	118.17	39.82	555.7	4.3	0.8	7.4	822.4	471.7	0.0	-2.7	76.6	62.9	-8.0	-69.4	1600
Baodiwang 4	117.34	39.55	198.8	50.6	6.9	38.8	384.3	92.9	163.2	-0.2	112.7	57.5	-9.7	-73.5	3000
Lizigu	117.34	39.52	220.2	56.3	7.2	34.8	384.3	124.4	177.9	-0.8	115.2	92.6	-9.1	-72.1	3000
Dijing	117.36	39.54	201.7	53.3	7.7	34.1	384.3	92.3	168.1	-0.4	112.6	82.2	-8.7	-71.2	—
Jixian	117.42	40.04	115.3	17.6	17.8	22.2	426.6	14.5	32.2	-0.8	72.5	27.5	-9.8	-69.3	—
Xinzhou 1	112.63	38.54	209.6	5.1	0.4	15.6	88.4	198.3	136.6	-0.9	89.8	46.3	-10.5	-77.3	—
Xinzhou 2	112.62	38.54	210.7	7.1	0.1	12.9	92.2	195.4	124.3	-0.4	111.2	56.9	-10.4	-77.1	—
Xinzhou 3	112.70	38.49	256.6	6.8	1.8	155.9	76.9	150.4	769.4	-3.1	77.1	46.0	-10.7	-80.3	—
Dingxiangtou	112.83	38.59	424.4	9.4	0.5	346.6	11.5	471.5	1510.1	-5.9	103.0	50.5	-11.3	-85.4	—
Yangouxiang	112.79	38.95	429.0	6.8	0.2	100.2	23.0	510.9	595.8	-4.0	108.5	40.3	-11.6	-87.0	—
Hunyuan	113.94	39.41	260.3	9.4	0.2	15.6	61.3	141.1	326.8	-1.5	114.4	63.8	-11.3	-88.2	—
Yanggao 1	113.82	40.42	109.9	5.2	2.4	18.1	165.2	64.1	56.2	0.6	67.5	39.6	-10.6	-79.7	172
Yanggao 2	113.82	40.42	114.6	4.2	2.5	14.4	153.7	63.6	62.2	0.9	62.1	39.7	-10.7	-81.6	203
Yanggao 3	113.82	40.41	87.1	4.6	3.4	19.3	149.9	38.2	44.1	1.2	60.5	45.9	-11.0	-81.6	—
Tianzhen 1	114.04	40.44	233.2	7.5	6.8	24.5	368.9	103.2	147.3	-0.2	63.9	43.8	-9.9	-80.5	504
Tianzhen 2	114.04	40.43	271.8	9.4	5.5	25.0	380.5	145.2	178.8	-0.8	71.7	42.8	-9.8	-81.5	100
Yuxian	114.44	39.80	46.5	3.6	40.5	72.5	361.2	26.5	81.1	0.2	31.1	11.4	-10.0	-74.5	—
Sanmafang	114.59	40.21	326.0	8.9	22.7	52.1	330.5	269.4	340.3	-1.8	54.6	39.4	-11.8	-88.5	180
Yangyuan	114.59	40.21	328.4	9.1	22.7	49.2	322.8	272.2	343.9	-1.9	55.1	39.1	-11.8	-88.6	—
Huailai 1	115.54	40.34	292.9	10.2	0.2	20.4	49.8	84.4	529.5	-2.3	121.6	75.0	-11.6	-89.3	—
Huailai 2	115.54	40.34	283.1	9.4	0.4	23.3	73.0	86.7	499.4	-1.9	104.3	47.2	-11.6	-88.0	—
Huailai 3	115.53	40.34	262.8	7.3	0.4	17.2	111.4	87.1	396.7	-1.1	98.4	47.2	-10.7	-83.2	288
Huailai 4	115.53	40.34	256.7	8.2	0.2	17.6	72.8	73.1	433.9	-2.4	109.7	66.0	-11.7	-88.8	500
Baimiaocun	115.40	40.66	179.9	3.8	2.0	12.6	134.5	34.2	238.4	-0.1	62.3	39.6	-11.5	-86.1	—
Dongwaikou	116.08	40.96	232.8	6.9	0.2	16.6	61.3	67.1	366.8	-1.5	109.9	56.0	-11.5	-87.6	—
Chicheng	115.74	40.90	203.0	8.2	0.8	32.4	115.3	29.0	403.5	-1.7	91.5	57.8	-12.0	-89.2	—
Shengshi	115.99	40.46	88.4	13.7	15.1	47.4	299.8	46.2	51.3	0.9	68.4	51.4	-11.5	-84.3	100
Songshan	115.82	40.51	143.6	2.8	0.2	9.6	57.3	35.6	177.2	-2.4	81.9	34.9	-11.9	-86.7	205
Wuliying	115.93	40.48	103.7	8.0	11.2	36.2	338.2	16.4	68.1	-0.5	59.8	29.3	-11.8	-86.0	553
Jinyu	115.97	40.48	85.5	13.0	15.2	46.8	299.8	44.4	48.4	0.8	67.2	42.8	-11.5	-84.2	—
Average			276.8	12.1	5.1	36.4	283.8	172.2	283.0		78.4				

— represent natural hot springs and self-flowing wells or well depth being not available.

orders of magnitude higher than that in air (0.03%). The concentration of CH_4 was low, ranging from 0 to 16.13%, with that in all samples below 1%, except for those of the Baodi, Lizigu, and Dijing springs.

The gas isotope data showed that the $^4He/^{20}Ne$ ratios ranged from 3.11 to 1,647, far exceeding that of air of 0.318. The R/Ra values of $^3He/^4He$ ranged from 0.01 to 2.52, representing typical mixtures of a crust and mantle source or radiogenic gas. The value of $\delta^{13}C$ in the samples ranged from −6.3‰ to −20.7‰.

5. Discussion

5.1. Helium and Neon Isotopes. Noble gases within the crust originate from three main sources [55]: (1) the atmosphere, introduced into the crust through groundwater recharge; (2) the mantle, from regions of magmatic activity; and (3) gases produced in the crust by the result of radioactive decay processes. The helium and carbon isotope ratios are sensitive tracers of gas sources due to varying gas isotope ratios among the atmosphere, crust, and mantle [25]. Helium is mainly derived from the atmosphere, crust, and mantle. The mixture of crust and mantle sources can be determined by the R/Ra ratio. The $^3He/^4He$ of atmospheric helium is 1.4×10^{-6}, known as Ra [56]. Previous studies on the R/Ra ratio of crustal helium provided slightly different but consistent values. For example, Poreda et al. [57] obtained a crustal R/Ra of 0.013–0.021, whereas Mamyrin and Tolstikhin [56] found that the crustal Ra was generally <0.05. The R/Ra of the mantle source generally exceeds 5; i.e., the R/Ra of $^3He/^4He$ is 7.9 [58], whereas White [59] obtained an R/Ra of 8.8 ± 2.5 for the upper mantle and 5–50 for the lower mantle. The R/Ra of the WZ13-1-1 natural gas well in the rift basin of the East China Sea is 8.8, which is the maximum Ra of any sedimentary basin in China [60, 61].

Table 3 shows the different ratios of $^3He/^4He$. The G1, G2, G3, G4, and G8 sampling points were characterized by helium isotopes from the crust with a $R/Ra < 0.1$. These sampling points were in the TNCB and close to the Ordos Basin. Other sampling points located in EB and TNCB showed different degrees of mantle-derived helium supply (Figure 3), consistent with the results of Zhang et al. [25].

The mantle source contribution of helium isotopes in gases of the hot springs ranged from 0 to 31.38%. The mantle source contributions of sampling locations G1, G2, G3, and G8 were below 0.5%. Sample location G8 was close to the Ordos Basin and represented a typical crustal source gas, with no mantle source contribution ($R/Ra = 0.01$). The sampling points G1, G2, and G3 s were in the Qicun geothermal field in Shanxi Province (Figure 1(b)). The Qicun geothermal field is in the Zhoushan fault-fold zone of Hongtaoshan-I in the Shanxi block of the North China Plate and is categorized as part of the plate interior thermal system. The heat source is vertical heat transfer through the crust, and the circulation of meteoric water occurs through deep faults [62, 63]. The mantle source contributions of sampling locations G6, G7, and G9 exceeded 10%, while those of sampling locations G12, G13, and G14 were 30.15%, 25.31%, and 31.38%, respectively. G9 is in the Houhaoyao thermal field, characterized by developed fractures and rock rupture, thus providing access and space for the upwelling of mantle-derived material [64]. The sampling locations G12, G13, and G14 are in the Yanhuai Basin (Figure 1(b)). The regional geophysical data showed the presence of typical crustal faults, magmatic activities, complex structural patterns composed of shallow faults, and a mantle transition zone in the lower part [65]. The hot spring gases distributed in the central NCC indicated the presence of mantle sources in the TNCB, which may be related to crustal thinning in the region. A low-speed belt of 130 km was noted at the junction between the northern North China Basin and the Yanshan orogenic belt. This belt experienced multiple periods of tectonic activities, thereby providing a favorable channel for gas upwelling [66, 67]. The TNCB is a typical continent-to-continent collision belt that was formed by the collision between the EB and the WB at ~1.85 billion years ago. The rock unit in the region experienced intense multistage deformations accompanied by large-scale overthrusting and ductile shear [68]. Tectonic activity, crustal thinning, and deep cut active faults provide good conditions for mantle gas emission. The high $^3He/^4He$ ratios (0.10–2.52 Ra) are associated with the injection of a magmatic reservoir beneath the fault in the TNCB and EB, and subduction of the Pacific Plate also results in higher activity in the TNCB and EB [69].

Typical crustal sources of helium isotopes in hot spring gases for sampling sites G1, G2, G3, G4, and G8 were distributed in the western EB, outside of the boundaries of the Ordos Basin. The remaining 21 hot spring sampling sites showed a mantle-derived gas supply, similar to the spatial scope of the destruction of the Pacific Plate subduction to the east of the NCC (Figure 3(b)). This assertion was further verified by Dai et al. [26] who found that helium isotopes of gas in the Ordos Basin were characterized by low CO_2 and low R/Ra values (<0.1) typical of the craton basin [72, 73].

The spatial differentiation of gas isotope sources is not accidental. Many fault basins were formed in the east NCC during the Paleogene. This was accompanied by long basalt eruptions and active magmatic activities. These events facilitated the formation of oil in the east NCC [69]. Besides, a low-velocity zone was observed at a depth of 70 km in the east NCC [66] along with an obvious lithosphere-asthenosphere boundary (LAB) [74]. These observations confirm the presence of deep fluid activity in the eastern NCC. The EB and the TNCB contain greater quantities of mantle-derived gases and more direct channels. The thickness of the lithosphere of the western Ordos Basin (80–180 km) exceeds that of the EB and the TNCB, and an area of thinning is evident to the east of the basin [75], characterized by less magmatic activity and a stable structure [7, 9]. The eastern NCC shows a higher heat flow compared to the western part [76], which can be related to magma activity during the late Mesozoic and thinning of the continental lithosphere.

5.2. Gas Composition. The present study analyzed 16 hot spring gas samples in the EB and TNCB (Table 3). All

Table 2: Sampling locations, water temperatures, reservoir temperatures, and chemical compositions in the Western block and the Trans-North China Block of the North China Craton.

Well no.	Longitude (°E)	Latitude (°N)	Na^+ (mg/L)	K^+ (mg/L)	Mg^{2+} (mg/L)	Ca^{2+} (mg/L)	HCO_3^- (mg/L)	Cl^- (mg/L)	SO_4^{2-} (mg/L)	IB (%)	$T_{K\text{-}Mg}$ (°C)	T (°C)
Shangwangtai	106.96	34.56	189.1	5.3	1.4	37.8	169.0	34.0	399.0	-1.9	73.7	28.5
Qianchuan	107.15	34.64	34.7	7.2	22.6	71.9	637.0	11.2	21.1	2.1	50.2	14.8
Shuigouzhen	106.99	34.74	8.1	1.0	15.5	60.4	452.0	3.4	13.1	2.1	—	17.1
Shenjiazui	106.89	34.85	22.4	3.3	20.3	100.0	634.0	12.9	50.5	0.7	35.8	14.8
Chaijiawa	106.77	34.94	5.3	1.3	23.5	55.8	518.0	2.4	7.6	1.4	—	17.9
Shilitan	106.40	35.43	17.0	1.4	20.0	71.4	601.0	9.4	37.2	-1.8	—	10.2
Dayuanzi	106.39	35.46	53.2	2.4	50.0	98.3	645.0	21.2	257.2	-1.0	—	11.4
Fujianchang	106.68	35.53	20.4	1.7	21.4	58.8	455.0	5.7	34.6	3.3	—	12.2
Liuhu	106.67	35.55	134.2	5.9	44.2	61.8	660.0	77.9	223.3	0.3	39.5	18.5
Beishan 1	106.70	35.56	84.8	1.2	25.9	33.9	619.0	15.9	44.6	2.3	—	13.7
Beishan 2	106.68	35.56	138.5	1.2	50.9	36.1	809.0	23.4	183.4	1.1	—	12.9
Baiyunsi 2	106.24	35.60	29.6	1.5	34.7	66.3	508.0	3.7	151.1	-0.3	—	12.1
Baiyunsi 1	106.25	35.61	41.3	3.0	39.5	66.5	445.0	6.2	212.9	0.1	27.8	10.9
Baiyunsi 3	106.25	35.61	31.3	1.7	34.7	52.1	436.0	3.3	129.0	1.3	—	17.3
Dongshanpo	106.28	35.62	262.6	1.9	0.7	2.4	1219.0	23.4	4.5	-0.7	59.4	10.2
Anguo 1	106.57	35.62	148.8	6.0	45.0	64.5	713.0	77.7	235.0	0.5	39.6	22.3
Anguo 2	106.57	35.62	170.1	6.9	43.9	61.1	688.0	97.2	269.7	-0.2	42.6	24.4
Longde	106.13	35.62	68.8	1.8	37.2	60.3	746.0	18.9	101.1	-0.1	—	13.8
Hongjunquan	106.18	35.67	52.5	2.0	36.2	79.9	545.0	3.5	228.5	-0.7	—	10.2
Heshangpu	106.23	35.68	22.4	2.2	33.5	58.2	519.0	6.7	111.0	-1.2	—	11.7
Beilianchi	106.18	35.74	25.5	1.8	31.1	44.7	475.0	2.6	66.8	1.6	—	20.0
Lianchisi	106.18	35.74	23.7	1.3	24.5	38.8	420.0	2.4	50.4	1.3	—	16.7
Fuxiya	106.17	35.75	4.3	1.8	1.2	31.6	199.0	1.2	4.1	0.0	52.0	19.0
Hongtai	105.79	35.76	731.8	5.8	199.4	142.7	689.0	256.6	1754.9	2.5	25.3	13.0
Wangminjing	105.74	35.80	1020.9	9.2	3.2	18.3	606.0	357.6	1313.2	1.7	77.5	11.9
Pengyang	106.63	35.85	134.1	4.5	52.7	62.1	684.0	78.3	240.7	0.3	33.0	18.2
Xiangyang	106.40	35.95	618.9	2.1	0.7	0.0	1131.0	31.7	1002.4	-1.8	60.3	22.4
Choushuihe 3	106.06	36.01	6861.9	25.2	122.7	264.3	1006.0	5057.4	11260.7	-4.5	58.7	17.1
Xiaokou 2	106.08	36.01	19817.0	116.1	28.2	138.1	2580.0	7759.8	30847.2	-0.3	116.4	17.6
Xiaokou 1	106.08	36.02	24462.5	156.5	90.7	220.1	1508.0	11018.9	37317.9	-0.4	108.1	8.8
Chaigou 2	105.88	36.07	135.1	2.7	55.6	108.5	717.0	22.4	484.7	-1.6	—	9.0
Chaigou	105.89	36.08	108.5	2.4	53.2	72.4	632.0	13.8	297.8	1.4	—	12.9
Heiyanquan	105.88	36.08	94.5	2.5	46.6	82.9	731.0	14.9	280.3	-1.1	—	10.4
Choushuihe 1	106.04	36.13	50.7	3.0	63.0	101.0	857.0	6.6	264.3	-1.0	—	17.1
Choushuihe 2	106.17	36.14	8210.0	27.1	144.9	340.0	1095.0	6007.2	13942.9	-4.8	58.5	17.8
Hongyang	105.64	36.26	300.3	3.5	92.7	499.1	112.0	152.0	2580.0	-6.3	—	11.0
Zhengqi	105.96	36.45	901.4	5.6	204.3	279.7	145.0	1918.4	1420.9	-4.7	—	12.4
Xiaoshanquan	105.60	36.50	15.7	4.3	32.6	59.8	523.0	6.8	69.1	1.3	36.6	13.1
Shuangjing	106.25	36.59	3598.0	184.1	91.0	318.8	1581.0	—	9313.4	-3.0	112.7	25.1
Ganyanchi	105.23	36.67	622.1	6.8	107.0	11.0	1524.0	735.1	846.6	-8.4	34.0	16.2
Yaoxian	105.17	37.41	510.3	10.8	117.3	133.1	435.0	660.3	1064.6	-3.7	41.8	17.7
Shuitaocun	106.31	37.46	452.4	4.5	146.1	123.2	478.0	695.8	900.4	-3.0	—	13.9
Nitanjing	105.20	37.46	602.3	7.3	9.2	48.2	29.0	629.6	474.4	1.4	60.1	19.4
Nitanquan	105.20	37.46	867.2	5.4	35.6	28.5	608.0	404.7	1516.4	-4.0	39.9	15.8
Daquan	106.34	37.97	105.4	1.2	16.1	14.4	248.0	72.8	90.9	2.1	—	17.6
Miaoshan 1	105.85	38.03	273.9	5.5	45.0	58.6	540.0	267.6	337.6	-0.8	38.1	15.4
Miaoshan 2	105.86	38.03	258.3	5.5	43.5	56.7	561.0	246.2	317.8	-1.0	38.4	17.3

Table 2: Continued.

Well no.	Longitude (°E)	Latitude (°N)	Na^+ (mg/L)	K^+ (mg/L)	Mg^{2+} (mg/L)	Ca^{2+} (mg/L)	HCO_3^- (mg/L)	Cl^- (mg/L)	SO_4^{2-} (mg/L)	IB (%)	$T_{K\text{-}Mg}$ (°C)	T (°C)
Hongshitou 1	105.67	38.76	116.2	2.7	41.9	68.0	334.0	174.2	186.9	-0.1	25.7	12.6
Hongshitou 2	105.68	38.77	160.7	5.0	34.1	58.1	425.0	148.2	238.6	-0.6	38.9	20.9
Dashuigou	106.15	38.89	16.2	2.0	14.2	68.4	346.0	13.3	59.9	2.0	29.7	12.8
Longquansi	106.28	38.96	53.6	2.8	19.5	53.4	358.0	52.8	105.5	-0.9	32.9	16.4
Jianquan	106.48	39.08	101.1	6.3	123.0	117.7	662.0	80.3	650.6	-1.0	31.1	18.4
Shitanjing 2	106.31	39.18	127.2	7.4	49.5	205.2	349.0	92.9	857.6	-4.1	42.8	23.9
Shitanjing 1	106.31	39.18	91.3	4.3	38.5	150.7	337.0	76.2	534.2	-2.6	34.9	13.5
Diyan	106.93	39.64	49.9	1.9	24.7	85.2	305.0	69.0	152.6	1.6	—	16.8
Subeigou	106.95	39.67	83.1	3.7	29.7	68.9	343.0	80.2	155.8	1.5	34.3	15.4
Qianligou 1	106.99	39.86	122.1	4.2	39.1	77.6	405.0	107.5	248.5	0.8	34.5	12.5
Qianligou 2	106.98	39.86	130.1	3.9	39.4	72.1	354.0	122.1	238.7	1.4	32.9	19.1
Dahuabei	109.41	40.73	9.7	2.2	9.5	68.0	426.0	9.3	37.1	-0.3	35.5	12.9
Hongqicun	109.33	40.73	15.4	1.9	16.6	80.6	514.0	13.6	34.7	1.0	27.2	11.4
Xishanzui	108.73	40.74	80.0	4.8	50.7	153.7	351.0	134.5	270.9	0.3	34.4	14.6
Aguimiao	106.42	40.74	50.0	3.5	27.5	62.3	379.0	48.2	109.5	0.7	34.0	15.1
Zhaoer	106.54	40.88	64.6	17.2	35.1	122.8	465.0	92.9	241.4	-0.4	64.2	19.2
Chendexi	106.53	40.88	71.6	29.8	37.4	126.8	454.0	125.4	248.3	-0.2	76.2	16.7
Shimen	106.56	40.88	75.5	13.4	42.8	99.9	443.0	81.6	303.4	-1.1	56.6	25.8
Chahangou	106.57	40.88	28.7	1.7	7.3	45.9	277.0	16.6	43.7	0.8	33.0	17.2
Buerdong	106.57	40.89	68.9	16.2	37.4	118.7	443.0	92.3	306.7	-0.8	62.1	27.8
Shaotoushan	109.14	41.12	69.5	2.6	59.1	61.5	589.0	56.2	165.6	1.9	—	17.3
Dongsheng 1	107.04	41.13	40.3	14.0	35.9	84.8	463.0	52.5	151.0	-0.1	59.4	13.3
Dongsheng 2	107.03	41.14	43.8	15.3	67.7	56.3	730.0	32.4	112.5	1.1	54.4	14.8
Xiliushu	107.93	41.28	42.4	2.2	15.6	58.8	401.0	19.1	73.1	0.1	30.8	14.7
Hulusitai	107.79	41.28	82.9	3.3	16.3	64.2	528.0	46.9	101.6	0.4	37.9	14.5
Yangguangcun	108.29	41.29	21.4	3.7	11.8	64.1	380.0	12.6	32.0	0.8	43.3	14.4
Xiremiao 2	108.66	41.54	51.0	2.1	28.5	86.4	658.0	40.1	78.8	0.7	—	23.7
Xiremiao 1	108.66	41.54	50.2	2.6	27.2	72.5	553.0	38.4	78.5	0.9	28.7	18.6
Xiremiao 3	108.66	41.54	44.4	1.6	28.3	69.8	572.0	35.7	75.0	0.0	—	16.5
Hailiutu	108.51	41.59	54.7	4.8	22.4	67.4	402.0	39.4	69.7	1.6	42.2	17.2
Average			965.7	11.1	45.3	92.0	589.3	505.0	1645.9		47.4	

— represents spring water not suitable for a cation temperature scale.

samples were rich in N_2 (69.42–98.52%). The content of N_2 of the gas samples was characteristic of that of a medium-low temperature hydrothermal system, such as the peninsula craton in the heat field of central and western India, indicating low deep equilibrium temperatures [77]. The accumulation of N_2 may be due to thermal decomposition of organic matter in sedimentary and metamorphic rocks [78].

The N_2/Ar ratios in air, air-saturated water (ASW), and groundwater were 84, 38, and 50, respectively [80–82]. The results of the present study showed a strong correlation between N_2 and Ar (Figure 4). Plotting the results of gas sample analysis showed two separated distributions. Gas samples were distributed along the He-air trend line with N_2/Ar ratios approaching that of air of 84, suggesting that N_2 originated from the atmosphere and that aquifers were recharged with meteoric water containing dissolved air. Atmospheric precipitation is the main source of Ar in geothermal gas [32]. Therefore, both Ar and N_2 in hot spring gas originated from the atmosphere.

The N_2/He ratios of 11 samples showed regional variation of sources. As shown in Figure 2, the sampling locations G1, G2, G3, and G4 showed crustal predominated gases, consistent with the results of the helium-neon isotope (Figure 5). The mantle source contribution of sampling locations G5, G6, G7, and G8 was significantly increased. These gas sampling points were in the central TNCB. Simultaneously, the sampling locations G9, G11, and G15 contained typical subduction zone gases. These sampling locations were in the EB which experienced the highest degree of destruction of the NCC. Arc-type gases are characterized by a high N_2 content, N_2/Ar ratios > 200, and N_2/He ratios > 1,000. Mantle-derived gases are characterized by a low N_2 content and N_2/He ratios < 200 [80]. Sample location G15 is in the Bohai Bay Basin in the Huanghua Depression

Table 3: Chemical and isotopic compositions of hot spring gases in the Eastern block and the Trans-North China Block of the North China Craton.

No.	Sampling site	Longitude (°E)	Latitude (°N)	N_2 (%)	O_2 (%)	Ar (%)	CO_2 (%)	CH_4 (%)	^4He (%)	$^4He/^{20}Ne$	R/Ra	Rc/Ra	He_M (%)	$\delta^{13}C_{PDB}$ (‰)	Tectonic unit
G1	Qicun	112.62	38.54	96.44	0.60	1.43	0.03	0.03	1.47	319.36	0.04	0.04	0.24	-14.3	TNCB
G2	Duncun	112.70	38.49	95.72	0.85	1.38	0.13	—	1.92	734.05	0.03	0.03	0.12	-18.2	TNCB
G3	Tangtou	112.83	38.59	92.12	2.72	1.47	0.07	0.05	3.58	971.09	0.03	0.03	0.12	-17.5	TNCB
G4	Yangou	112.79	38.95	91.25	3.31	1.41	0.01	0.03	3.99	1647.60	0.07	0.07	0.62	-18.6	TNCB
G5	Hunyuan	113.94	39.41	96.79	1.19	1.45	0.01	0.10	0.46	188.65	0.62	0.62	7.51	-17.5	TNCB
G6	Shengshui	114.04	40.44	89.90	6.65	1.30	1.84	—	0.31	149.34	1.02	1.02	12.53	-15.0	TNCB
G7	Tianzhen	114.04	40.43	94.45	2.84	1.31	1.00	—	0.41	219.28	0.99	0.99	12.16	-14.5	TNCB
G8	Yangyuan	114.59	40.21	96.10	1.31	1.25	0.98	0.02	0.34	185.52	0.01	0.01	0	-15.4	TNCB
G9	Houhaoyao	115.54	40.34	88.33	9.35	1.31	0.01	0.91	0.09	202.85	0.96	0.96	11.78	-20.7	TNCB
G10	Dongwaikou	116.08	40.96	N.A.	N.A.	N.A.	N.A.	N.A.	N.A.	135.54	0.49	0.49	5.88	-16.1	TNCB
G11	Tangquan 1	115.74	40.90	N.A.	N.A.	N.A.	N.A.	N.A.	N.A.	85.42	0.42	0.42	4.99	-16.1	TNCB
G12	Shengshiyuan	115.99	40.46	N.A.	N.A.	N.A.	N.A.	N.A.	N.A.	63.15	2.42	2.43	30.15	-12.7	TNCB
G13	Wuliying	115.93	40.48	N.A.	N.A.	N.A.	N.A.	N.A.	N.A.	28.83	2.03	2.04	25.31	-14.2	TNCB
G14	Jinyu	115.97	40.48	N.A.	N.A.	N.A.	N.A.	N.A.	N.A.	96.07	2.52	2.52	31.38	-13.1	TNCB
G15	Liyuantou	117.19	39.03	N.A.	N.A.	N.A.	N.A.	N.A.	N.A.	155.30	0.27	0.27	3.12	-19.8	EB
G16	Xiawucun	117.78	39.27	N.A.	N.A.	N.A.	N.A.	N.A.	N.A.	14.70	0.19	0.18	1.95	-20.6	EB
G17	Luqiancun	117.78	39.29	96.65	1.90	1.30	0.14	0.02	—	3.11	0.16	0.08	0.78	-20.7	EB
G18	Zunhua	117.76	40.21	98.52	0.07	1.28	0.05	0.01	0.08	41.81	0.42	0.42	4.97	-17.2	EB
G19	Jidong	118.34	39.18	N.A.	N.A.	N.A.	N.A.	N.A.	N.A.	8.12	0.34	0.32	3.73	-18.0	EB
G20	Liuzan	118.68	39.16	N.A.	N.A.	N.A.	N.A.	N.A.	N.A.	211.95	0.35	0.35	4.13	-17.4	EB
G21	Changsheng	118.17	39.82	N.A.	N.A.	N.A.	N.A.	N.A.	N.A.	538.73	0.70	0.70	8.52	-17.2	EB
G22	Baodi	117.34	39.55	69.42	5.30	1.09	7.91	16.13	—	44.50	0.49	0.49	5.85	-9.3	EB
G23	Lizigu	117.34	39.52	74.55	18.57	1.05	2.19	3.60	—	17.80	0.47	0.46	5.54	-9.8	EB
G24	Dijing	117.36	39.54	73.88	17.20	0.92	5.55	2.45	—	85.63	0.48	0.48	5.74	-6.4	EB
G25	Jingdong	116.94	39.96	95.78	1.60	1.29	0.72	0.54	0.07	82.53	0.16	0.16	1.72	-14.4	EB
G26	Huashuiwan	116.50	40.18	97.19	0.13	1.21	1.74	0.03	—	20.65	0.54	0.53	6.44	-11.20	EB

"—" stands for contributions below 0.1%. N.A.: not analyzed. $\delta^{13}C$ is the value of CO_2 in the analyzed sample.

and Cangxian uplift area. This area has conditions that facilitate mantle degassing. The mantle source contributions of the sampling points gradually increased from west to east (Figure 3(b)), and the gas characteristics of the subduction zone were observed in the EB (Figure 4).

5.3. Carbon Isotopes of CO_2. CO_2 in hot spring gas is generated by the organic or inorganic process. The formation of CO_2 through organic processes involves the decomposition of organic matter and bacterial activities. Formation of CO_2 through inorganic processes involves magmatic activities in the mantle, thermal decomposition, and the dissolution of carbonate rocks [83]. The $\delta^{13}C$ value is an effective criterion to determine the source of carbon dioxide and methane [84]. $\delta^{13}C$ in CO_2 for degassing of the upper mantle ranges from −8‰ to −4‰ [85, 86]. The values of $\delta^{13}C_{CO2}$ with a magmatic origin range from −9.1‰ to 2‰ [87, 88]. $\delta^{13}C_{CO2}$ in sedimentary basins is generally regulated by the generation of organic hydrocarbon by thermal decomposition and ranges from −15‰ to −25‰ [89]. $\delta^{13}C_{CO2}$ of organic origin is generally lower than −10‰, while $\delta^{13}C_{CO2}$ of inorganic origin typically ranges from −8‰ to 3‰ [90].

Figure 6 shows the mixing of different sources. The $\delta^{13}C_{CO2}$ isotope showed a trend indicative of depositional genesis of carbonates (dashed box). Carbonate rocks account for 80% of the volume of sedimentary strata in the region and provide a material source for carbon [37]. Only the $\delta^{13}C_{CO2}$ of sampling locations G22, G23, and G24 exceeded −10‰. These sampling locations were in the central North China Plain (EB). Meanwhile, the CO_2 concentration of spring water was relatively low, ranging from 0.01 to 7.91%. The CO_2 concentrations of only sampling locations G22, G23, and G24 exceeded 2% (Table 3). Most organic carbon was observed in the EB, and the $\delta^{13}C_{CO2}$ value of sedimentary origin in the EB was similar to that in the Ordos Basin (Figure 6).

The CO_2 concentrations in the samples observed in the present study were different from those of gas wells recorded by Dai et al. [26] in the Ordos Basin of 0.02–8.87% with an average of 1.86%. The maximum value and average CO_2 concentrations in the Bohai Bay Basin far exceeded those in the Ordos Basin, with an average value of >10%. This observation could be attributed to the dissolution of CO_2 in water being promoted by the high temperature of geothermal water, leaving behind only a small quantity of inorganic carbon.

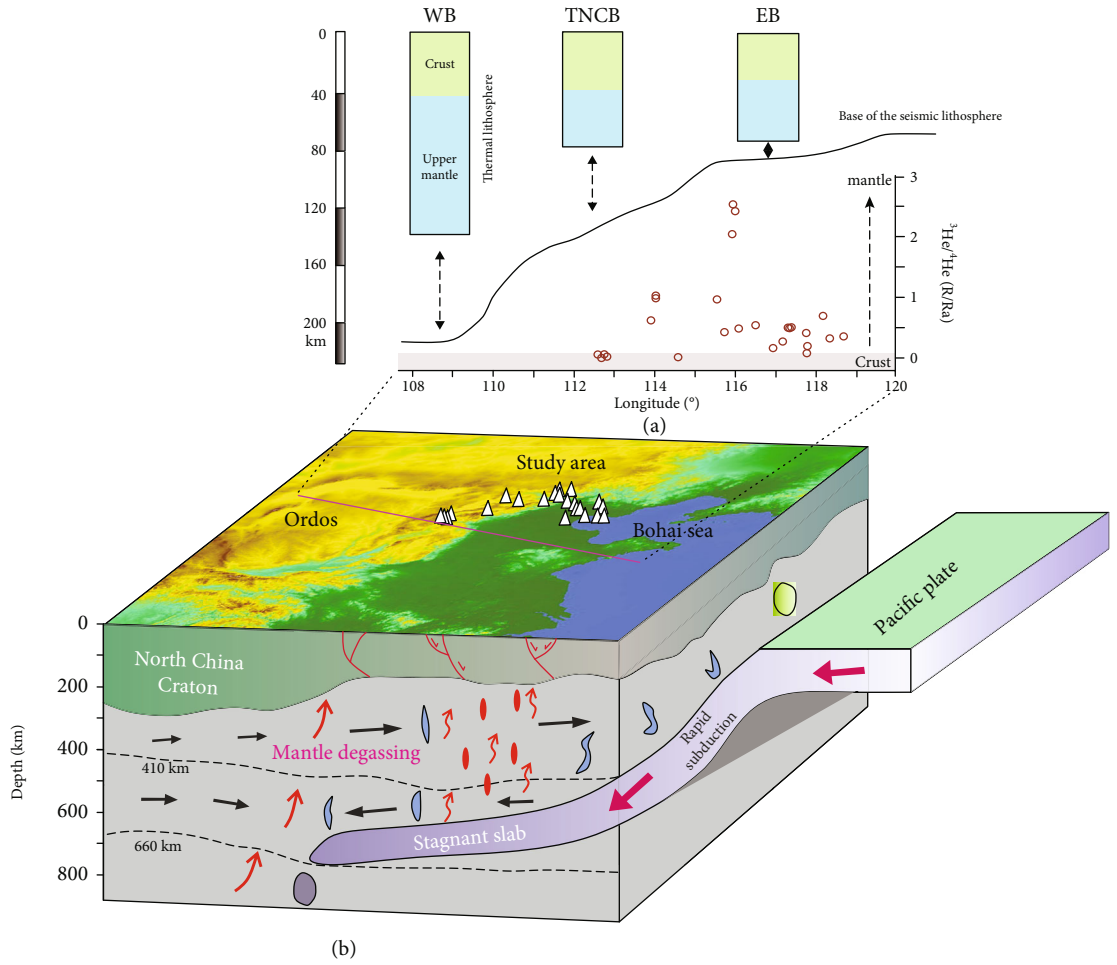

Figure 3: Conceptual model of He isotopes in the North China Craton (NCC). (a) Comparison between the thermal and seismic lithospheric bases for the NCC and the ^{3}He/^{4}He (Ra) of the Eastern Block (EB) and the Trans-North China Block (TNCB) [70]. (b) The mantle convection regime for the destruction and modification of the lithosphere beneath the NCC, as modified after Zhu et al. [7]. Faults according to Chen et al. [71].

Moreover, ^{3}He/^{4}He (R/Ra) showed that gas in the sample sites near the EB was of mantle origin. In contrast, the gas component in the sample sites near the Ordos Basin was of sedimentary origin (Figure 6).

5.4. Hydrogen and Oxygen Isotopes. Stable isotopes of hydrogen and oxygen can be used to identify the geothermal water source, trace the circulation path, and analyze the geothermal reservoir environment [37, 92]. There are significant differences in the hydrogen and oxygen isotopes among geothermal water, groundwater, meteoric water, and mixed water. The analysis of hydrogen and oxygen isotope ratios of meteoric water samples at different latitudes globally has shown that they all follow a linear relationship called the global meteoric water line (GMWL): $\delta D = 8\delta^{18}O + 10$ [93].

The average values of δD and δ^{18}O at the 46 sampling points in the study area were −78.46‰ and −10.27‰, respectively, and ranged from −77.26 to −69.27‰ and from −10.45 to −8.04‰, respectively. As shown in Figure 7, when plotting δD against δ^{18}O, most of the hydrogen and oxygen isotopes were distributed near the LMWL, indicating a meteoric water source. The results indicated oxygen shifting, with a maximum shift of 1.39 (G21).

Rocks are rich in oxygen (>40%) and poor in hydrogen (less than 1%) [94]. Therefore, the occurrence of reactions between water and rocks can result in an oxygen shift in water, whereas δD remains largely stable. For example, the water-rock interaction between atmospheric precipitation and media containing carbonate water can enhance the δ^{18}O value of water [95]. A high temperature can promote interactions between water and rock, thereby intensifying the exchange of oxygen isotopes between geothermal water and oxygen-enriched surrounding rock. The δD and δ^{18}O of Tianzhen 1 in the TNCB were −9.8‰ and −81.5‰, whereas those of Tianzhen 2 were −9.9‰ and −80.5‰, respectively. These results indicate that the exchange of oxygen isotopes may occur in the presence of oxygen-rich rocks in the quaternary sand-gravel aquifer of the Yanggao-Tianzhen Basin [25]. The δ^{18}O values span a wide range (−10.3 to −8.0‰), and it is noteworthy that the samples all plot to the right of the GMWL, with relatively uniform δD values. By considering an average isotopic gradient of precipitation for China, it can be concluded from the H and

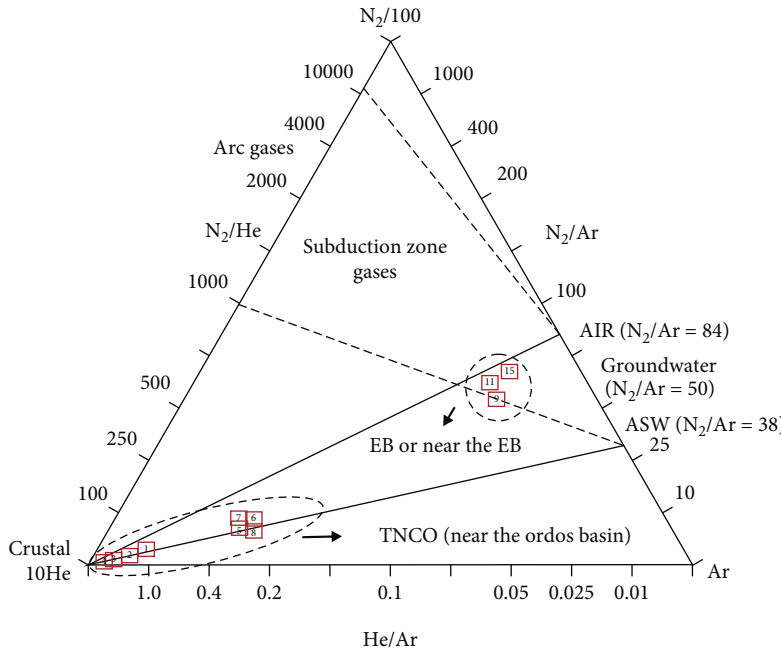

Figure 4: Relative N_2-He-Ar abundances in free gas. The ASW represents air-saturated water [79]. Classification of subduction-derived gases after Fischer et al. [80]. Numbers and names of sampling sites are listed in Table 3.

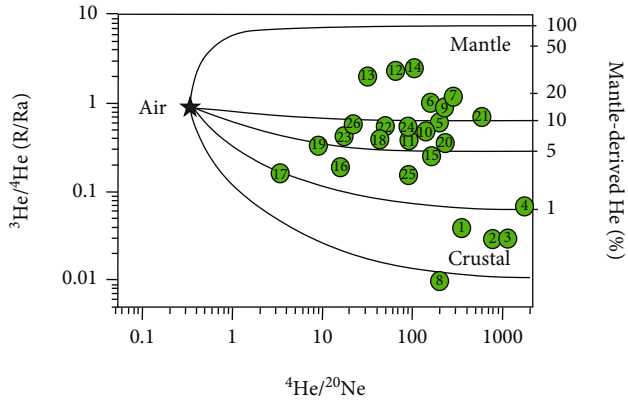

Figure 5: Plot of R/R_a-$^4He/^{20}Ne$ in the Trans-North China Block (TNCB) and Eastern Block (EB). Endmembers in the plot are $(R/R_a)_{air} = 1$, $(^4He/^{20}Ne)_{air} = 0.254$, $(R/R_a)_{mantle} = 8$, $(^4He/^{20}Ne)_{mantle} = 1000$, $(R/R_a)_{crust} = 0.02$, and $(^4He/^{20}Ne)_{crust} = 1000$ [91]. Numbers and names of sampling sites are listed in Table 3.

O isotopes that probably the difference of $\delta^{18}O$ is due to the fact that the geothermal water is recharged from different areas, the Taihangshan Range and Yan Shan Range NW of Tianjin [96]. Meanwhile, $\delta^{13}C_{CO2}$ in the EB is of carbonate sedimentary origin (Figure 6), thereby facilitating oxygen isotope exchange in water-rock reactions. The corresponding δD and $\delta^{18}O$ values of magmatic water are $-20 \pm 10‰$ and $10 \pm 2‰$, respectively [97, 98]. In addition, the δD and $\delta^{18}O$ of the EB exceeded those of the WB (Figure 7), possibly due to magmatism.

There were obvious spatial differences in δD between the EB and TNCB. The average δD values of the EB and TNCB were −79.2‰ and −84.1‰, respectively, significantly lower than those in the area of destruction in the NCC. The δD value can be used to derive the groundwater recharge depth in the crust, which decreases with the depth [99]. The results of reservoir temperature and δD indicated that the EB has deeper groundwater circulation. Moreover, the contribution of deep mantle heat flow in the eastern NCC exceeds that in the western NCC [14]. This result may be related to active underground magmatic activity in the eastern NCC, the thinning of the crust, and the higher intensity of seismic activity.

5.5. Reservoir Temperature in the NCC. Shallow geothermal data are of great significance for describing thermal states and revealing geodynamic processes of the continental lithosphere [100–102]. Since water-rock reactions are related to temperature, the geochemical thermometer has been widely used to estimate the final temperature of the water-rock balance in a reservoir [103]. Na-K-Mg trigonometry is usually used to determine the degree of water-rock reaction balance [104]. The Na-K-Mg trigonometry diagram is largely used to study hydrothermal systems and can provide a basis for chemical geothermometers [105].

The results of the present study showed that the geothermal water in the Ordos Basin was largely local equilibrium water, whereas most of the geothermal water in the EB was immature (Figure 8). The present study used the cation temperature scale to calculate the reservoir temperature. The prerequisite for using the temperature scale should be as follows: water should be in equilibrium, temperature should be greater than 25°C, and the calculated reservoir temperature should exceed the measured temperature when using the thermometric scale to calculate the reservoir temperature

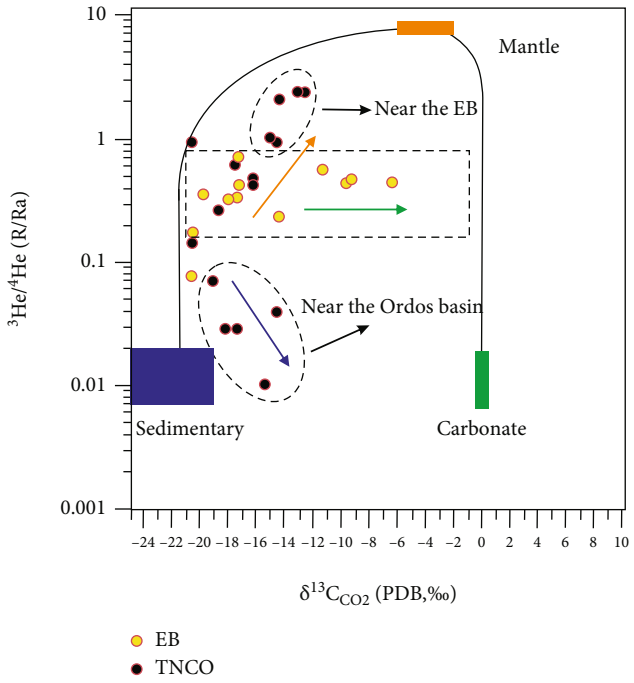

Figure 6: Plot of $^3He/^4He$ (R/Ra) vs. $\delta^{13}C_{CO2}$. The endmember compositions for sedimentary organic carbon (S, $\delta^{13}C_{CO2} = -25‰ - -19‰$, $^3He/^4He$ (R/Ra) = 0.01; green arrow), mantle carbon (M, $\delta^{13}C_{CO2} = -6‰ - -2‰$, $^3He/^4He$ (R/Ra) = 8; orange arrow), and limestones (L, $\delta^{13}C_{CO2} = 0‰$, $^3He/^4He$ (R/Ra) = 0.01; blue arrow) [91]; numbers and names of sampling sites are listed in Table 3.

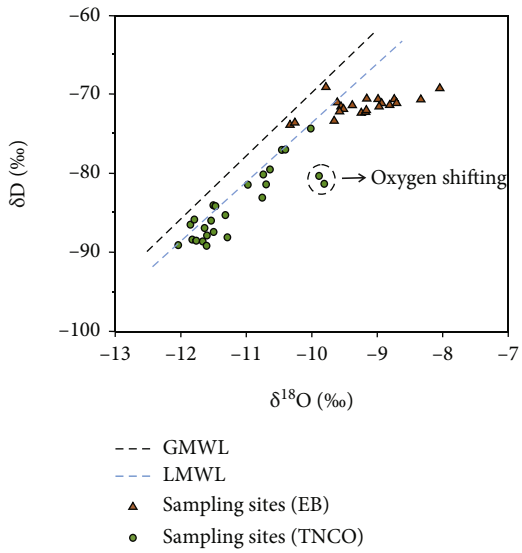

Figure 7: Hydrogen and oxygen stable isotopic composition of geothermal water in the Eastern Block (EB) and the Trans-North China Block (TNCB) of the North China Craton (NCC). GMWL stands for global meteoric water line: $\delta D = 8\delta^{18}O + 10$ [93]; LMWL stands for local meteoric water line, which is the meteorite water line of the monsoon region of Eastern China: $\delta D = 7.46\delta^{18}O + 0.9$ [106]. Numbers and names of sampling sites are listed in Table 1.

of a hot spring. Although some spring water in the study area does not apply to these temperature scales, there were differences in the calculated reservoir temperature between the EB and the WB, which are of reference significance. The K-Mg thermometric scale [104] can indicate the medium and low reservoir temperatures:

$$t^{\circ}C = \frac{4410}{14.0 - \log_{K2/Mg}} - 273.15. \quad (5)$$

The results of the K-Mg thermometric scale showed that the geothermal reservoir temperature of the WB ranged from 25.3 to 116.4°C, with an average temperature of 38.4°C, whereas the geothermal reservoir temperature in the EB and TNCB ranged from 31.1 to 112.6°C, with an average of 80.7°C (Figure 2; Tables 1 and 2). The present study used Inverse Distance Weighting (IDW) to analyze the spatial distribution of reservoir temperature. The IDW interpolation method is widely used in digital elevation models (DEMs), meteorological and hydrological analysis, and other fields due to its simplicity and convenient calculation [107].

The temperatures of hot springs in the WB ranged from 8.8 to 28.5°C, with an average of 16.1°C, whereas that in the EB and TNCB ranged from 11.4 to 92.6°C, with an average of 50.2°C (Tables 1 and 2).

Such regional differences are not accidental. The Ordos Basin has a crust with a temperature that exceeds that of the mantle and a mantle heat flow of 21.2–24.5 $mW{\cdot}m^{-2}$ [108]. The EB has a thermal state of mantle temperature that exceeds the temperature of the crust and a mantle heat flow ranging between 30 and 140 $mW.m^{-2}$, with an average of $61.9 \pm 14.8\,mW \cdot m^{-2}$ (He et al., 2011). The heat flow in the WB is related to a thicker lithosphere composed of continental blocks. In addition, the Cenozoic tectonic-thermal activity in the WB is weaker than that in the EB [70]. This can be attributed to the subduction of the Pacific Plate to the EB area, resulting in a thinner lithosphere and higher volcanic activity.

The inconsistency between measured temperatures and reservoir temperatures of hot springs can be partially attributed to the difference in heat flow (Figure 9) between the EB and the WB. Meanwhile, geothermal water circulation in the eastern NCC occurs at a greater depth. Crustal circulation at a greater depth is also a source of heat.

6. Conclusions

The TNCB and EB of the NCC provide paths for the emission of gas due to the presence of active faults. Continuous upwelling of mantle-derived gas occurs in the asthenosphere beneath the crust. The present study conducted a chemical analysis of the hot springs and gas in the craton basin as well as an isotope analysis in the EB and the TNCB, whereas a chemical analysis of hot springs was conducted in the WB. From the results of the present study, the following conclusions could be made:

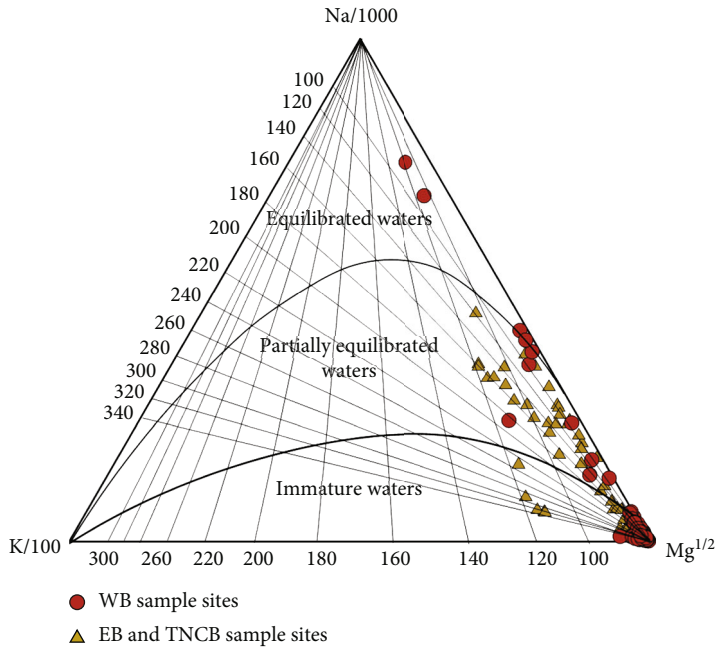

Figure 8: Na-K-Mg triangular diagram of geothermal waters of the North China Craton (NCC) (base map according to [104]).

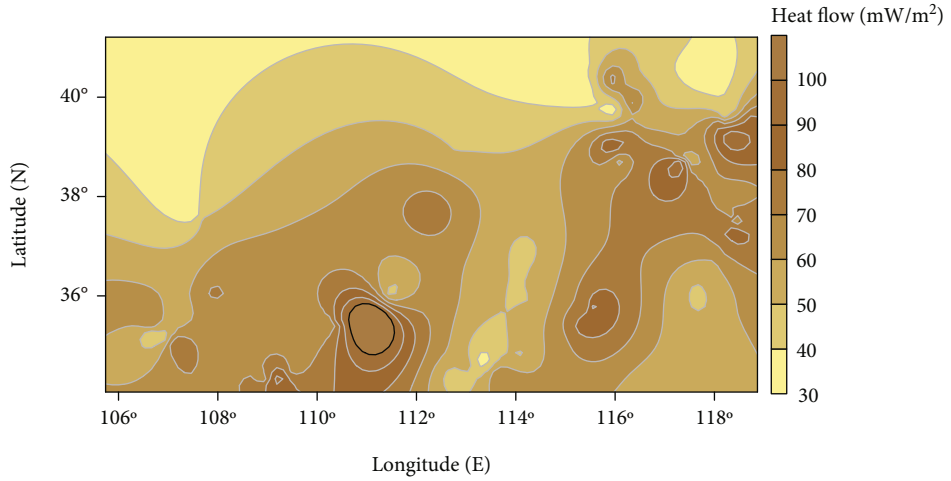

Figure 9: Contour map of heat flow in the North China Craton (NCC). Data from the China Heat Flow Database (CHFDB, chfdb.xyz).

(1) The compositions of helium-neon isotopes showed that mantle sources contributed to isotope compositions to different degrees in both the Bohai Bay Basin (EB) and the basin-ridge tectonic area (TNCB). There was a small mantle contribution of helium in Xinzhou near the Taihang Mountain. Moreover, the R/Ra of helium in most natural gas components of the Ordos Basin indicated crustal sources

(2) Abundant N_2 was noted in all hot springs in the eastern region, and the contribution of N_2 from mantle sources increased from west to east. Typical subduction zone gases were noted in the eastern region, which remained exposed in the Huailai Basin. Ar and N_2 in the study area may be of the same origin. The results of $\delta^{13}C_{CO2}$ showed that CO_2 in the gas in the EB is of organic origin, whereas that in the high-temperature geothermal area in some carbonate sedimentary layers was of inorganic origin

(3) The results of hydrogen and oxygen isotope analysis showed that the geothermal water in the east of the craton was meteoric water. δD increased gradually from west to east, whereas the depth of groundwater circulation increased. The temperatures of the thermal reservoir and water calculated by the ion temperature scale of the hot spring showed that the temperature of the EB far exceeded that in the WB.

Hydrochemistry, gas composition, and isotope analysis of hot springs in the NCC area can provide favorable evidence for the development and utilization of geothermal

fields. The results of the present study showed obvious spatial differences in these attributes, which could be related to tectonic conditions, magmatic activities, and active faults. Mantle-derived helium was found in the hot spring gas of the TNCB, consistent with the extent of Pacific Plate subduction.

Data Availability

The data supporting the findings of this study have been listed in the table in the paper.

Conflicts of Interest

The authors declare that they have no conflicts of interest.

Acknowledgments

Funding was provided by the Natural Science Foundation of China (No. 42073063), the National Key Research and Development Program of China (No. 2019YFC1509203), the Open Foundation of the United Laboratory of High-Pressure Physics and Earthquake Science (2019HPPES07), and the Basic Science Research Plan of the Institute of Earthquake Science, China Earthquake Administration (2020IEF0704, 2021IEF0707, and 2021IEF1205).

References

[1] D. G. Pearson, "The age of continental roots," *Lithos*, vol. 48, no. 1-4, pp. 171–194, 1999.

[2] R. L. Rudnick and D. M. Fountain, "Nature and composition of the continental crust: a lower crustal perspective," *Reviews of Geophysics*, vol. 33, no. 3, pp. 267–309, 1995.

[3] R. W. Carlson, D. G. Pearson, and D. E. James, "Physical, chemical, and chronological characteristics of continental mantle," *Reviews of Geophysics*, vol. 43, no. 1, article RG1001, 2005.

[4] M. Santosh, "Assembling North China Craton within the Columbia supercontinent: the role of double-sided subduction," *Precambrian Research*, vol. 178, no. 1-4, pp. 149–167, 2010.

[5] Y. J. Tang, H. F. Zhang, J. F. Ying, and B. X. Su, "Widespread refertilization of cratonic and circum-cratonic lithospheric mantle," *Earth Science Reviews*, vol. 118, pp. 45–68, 2013.

[6] F. Y. Wu, J. H. Yang, Y. G. Xu, S. A. Wilde, and R. J. Walker, "Destruction of the North China Craton in the Mesozoic," *Annual Review of Earth and Planetary Sciences*, vol. 47, no. 1, pp. 173–195, 2019.

[7] R. X. Zhu, L. Chen, F. Y. Wu, and J. L. Liu, "Timing, scale and mechanism of the destruction of the North China Craton," *China Earth Sciences*, vol. 54, no. 6, pp. 789–797, 2011.

[8] R. X. Zhu and Y. G. Xu, "The subduction of the west Pacific Plate and the destruction of the North China Craton," *Science China Earth Sciences*, vol. 62, no. 9, pp. 1340–1350, 2019.

[9] R. X. Zhu, Y. G. Xu, G. Zhu, H. F. Zhang, Q. K. Xia, and T. Y. Zheng, "Destruction of the North China Craton," *Science China Earth Sciences*, vol. 55, no. 10, pp. 1565–1587, 2012.

[10] W. L. Griffin, Z. Andi, S. Y. O'Reilly, and C. G. Ryan, "Phanerozoic evolution of the lithosphere beneath the Sino-Korean craton," *Mantle Dynamics and Plate Interactions in East Asia*, vol. 27, pp. 107–126, 1998.

[11] F. X. Lu, J. P. Zheng, R. S. Zhang, and M. H. Chen, "Phanerozoic mantle secular evolution beneath the eastern North China Craton," *Earth Science Frontiers*, vol. 12, pp. 61–67, 2005.

[12] Q. C. Fan and P. R. Hooper, "The mineral chemistry of ultramafic xenoliths of Eastern China: implications for upper mantle composition and the paleogeotherms," *Journal of Petrology*, vol. 30, no. 5, pp. 1117–1158, 1989.

[13] N. S. Qiu, Y. H. Zuo, J. Chang, and W. Z. Li, "Geothermal evidence of Meso-Cenozoic lithosphere thinning in the Jiyang sub-basin, Bohai Bay Basin, eastern North China Craton," *Gondwana Research*, vol. 26, no. 3-4, pp. 1079–1092, 2014.

[14] L. Y. Zhang, Q. Y. Liu, and L. J. He, "The different lithospheric thermal structure of North China Craton and its implications," *Chinese Journal of Geophysics*, vol. 59, pp. 3618–3626, 2016, (in Chinese with Enligsh abstract).

[15] Y. L. Kong, Z. H. Pang, H. B. Shao, S. B. Hu, and O. Kolditz, "Recent studies on hydrothermal systems in China: a review," *Geothermal Energy*, vol. 2, no. 1, pp. 1–12, 2014.

[16] E. R. Oxburgh and R. K. O'Nions, "Helium loss, tectonics, and the terrestrial heat budget," *Science*, vol. 237, no. 4822, pp. 1583–1588, 1987.

[17] D. M. Saffer, "The permeability of active subduction plate boundary faults," *Geofluids*, vol. 15, no. 1-2, p. 215, 2015.

[18] W. Ji-Yang, C. Mo-Xiang, W. Ji-An et al., "Geothermal studies in China," *Journal of Volcanology and Geothermal Research*, vol. 9, no. 1, pp. 57–76, 1981.

[19] L. J. Crossey, K. E. Karlstrom, A. E. Springer, D. Newell, D. R. Hilton, and T. Fischer, "Degassing of mantle-derived CO2 and He from springs in the southern Colorado plateau region–neotectonic connections and implications for groundwater systems," *Geological Society of America Bulletin*, vol. 121, no. 7-8, pp. 1034–1053, 2009.

[20] K. Bräuer, H. Kämpf, and G. Strauch, "Earthquake swarms in non-volcanic regions: what fluids have to say," *Geophysical Research Letters*, vol. 36, no. 17, article L17309, pp. 1–5, 2009.

[21] B. M. Kennedy and M. C. van Soest, "Flow of mantle fluids through the ductile lower crust: helium isotope trends," *Science*, vol. 318, no. 5855, pp. 1433–1436, 2007.

[22] L. Ma, M. C. Castro, and C. M. Hall, "Atmospheric noble gas signatures in deep Michigan Basin brines as indicators of a past thermal event," *Earth and Planetary Science Letters*, vol. 277, no. 1-2, pp. 137–147, 2009.

[23] J. D. Muirhead, T. P. Fischer, S. J. Oliva et al., "Displaced cratonic mantle concentrates deep carbon during continental rifting," *Nature*, vol. 582, no. 7810, pp. 67–72, 2020.

[24] Y. Sano, T. Hara, N. Takahata et al., "Helium anomalies suggest a fluid pathway from mantle to trench during the 2011 Tohoku-Oki earthquake," *Nature Communications*, vol. 5, no. 1, p. 3084, 2014.

[25] W. B. Zhang, J. du, X. C. Zhou, and F. Wang, "Mantle volatiles in spring gases in the Basin and Range Province on the west of Beijing, China: constraints from helium and carbon isotopes," *Journal of Volcanology and Geothermal Research*, vol. 309, pp. 45–52, 2016.

[26] J. X. Dai, Y. Y. Ni, S. F. Qin et al., "Geochemical characteristics of He and CO_2 from the Ordos (cratonic) and Bohaibay (rift) basins in China," *Chemical Geology*, vol. 469, pp. 192–213, 2017.

[27] S. Xu, G. D. Zheng, X. B. Wang, H. L. Wang, S. Nakai, and H. Wakita, "Helium and carbon isotope variations in Liaodong Peninsula, NE China," *Journal of Asian Earth Sciences*, vol. 90, pp. 149–156, 2014.

[28] S. L. Klemperer, B. M. Kennedy, S. R. Sastry, Y. Makovsky, T. Harinarayana, and M. L. Leech, "Mantle fluids in the Karakoram fault: helium isotope evidence," *Earth and Planetary Science Letters*, vol. 366, pp. 59–70, 2013.

[29] T. Yokoyama, S. Nakai, and H. Wakita, "Helium and carbon isotopic compositions of hot spring gases in the Tibetan Plateau," *Journal of Volcanology and Geothermal Research*, vol. 88, no. 1-2, pp. 99–107, 1999.

[30] G. Z. Sun, S. W. Liu, M. Santosh, L. Gao, Y. L. Hu, and R. R. Guo, "Thickness and geothermal gradient of Neoarchean continental crust: inference from the Southeastern North China Craton," *Gondwana Research*, vol. 73, pp. 16–31, 2019.

[31] G. C. Zhao, S. A. Wilde, P. A. Cawood, and M. Sun, "Archean blocks and their boundaries in the North China Craton: lithological, geochemical, structural and *P–T* path constraints and tectonic evolution," *Precambrian Research*, vol. 107, no. 1-2, pp. 45–73, 2001.

[32] J. M. Pang, Z. H. Pang, M. Lv, J. Tian, and Y. L. Kong, "Geochemical and isotopic characteristics of fluids in the Niutuozhen geothermal field, North China," *Environmental earth sciences*, vol. 77, no. 1, pp. 1–21, 2018.

[33] Y. H. Zuo, N. S. Qiu, Y. Zhang et al., "Geothermal regime and hydrocarbon kitchen evolution of the offshore Bohai Bay Basin, North China," *AAPG Bulletin*, vol. 95, no. 5, pp. 749–769, 2011.

[34] M. B. Allen, D. I. M. Macdonald, Z. Xun, S. J. Vincent, and C. Brouet-Menzies, "Early Cenozoic two-phase extension and late Cenozoic thermal subsidence and inversion of the Bohai Basin, northern China," *Marine and Petroleum geology*, vol. 14, no. 7-8, pp. 951–972, 1997.

[35] Q. Jin, G. Q. Song, H. B. Liang, F. Q. Cheng, and L. Wang, "Characteristics of carboniferous-Permian coal-derived gas in the Bohai Bay Basin and their implication to exploration potential," *Acta Geologica Sinica*, vol. 83, pp. 861–867, 2009, (in Chinese with English abstract).

[36] J. L. Mercier, P. Vergely, Y. Q. Zhang, M. J. Hou, O. Bellier, and Y. M. Wang, "Structural records of the late Cretaceous-Cenozoic extension in Eastern China and the kinematics of the southern Tan-Lu and Qinling Fault Zone (Anhui and Shaanxi provinces, PR China)," *Tectonophysics*, vol. 582, pp. 50–75, 2013.

[37] C. Lu, Y. Li, Z. Chen, and J. Yang, "A primary study on geochemical characteristics and genesis of geothermal water in the north-central part of the North China downfaulted basin," *Bull. Mineral Petroleum Geochemistry*, vol. 37, pp. 663–673, 2018, (in Chinese with English abstract).

[38] Z. Pang, J. Pang, Y. Kong, and L. Luo, "Large karstic geothermal reservoirs in sedimentary basins in China: genesis, energy potential and optimal exploitation," in *Proceedings World Geothermal Congress 2015*, Melbourne, Australia, 2015.

[39] X. W. Xu and X. Y. Ma, "Geodynamics of the Shanxi rift system, China," *Tectonophysics*, vol. 208, no. 1-3, pp. 325–340, 1992.

[40] J. L. Ma and Y. G. Xu, "Old EMI-type enriched mantle under the middle North China Craton as indicated by Sr and Nd isotopes of mantle xenoliths from Yangyuan, Hebei Province," *Chinese Science Bulletin*, vol. 51, no. 11, pp. 1343–1349, 2006.

[41] Y. G. Xu, J. Blusztajn, J. L. Ma, K. Suzuki, J. F. Liu, and S. R. Hart, "Late Archean to early Proterozoic lithospheric mantle beneath the western North China Craton: Sr-Nd-Os isotopes of peridotite xenoliths from Yangyuan and Fansi," *Lithos*, vol. 102, no. 1-2, pp. 25–42, 2008.

[42] W. Guangcai, Z. Zuochen, W. Min, C. A. Cravotta, and L. Chenglong, "Implications of ground water chemistry and flow patterns for earthquake studies," *Ground Water*, vol. 43, no. 4, pp. 478–484, 2005.

[43] X. Y. Xie and P. L. Heller, "U-Pb detrital zircon geochronology and its implications: the early late Triassic Yanchang formation, south Ordos Basin, China," *Journal of Asian Earth Sciences*, vol. 64, pp. 86–98, 2013.

[44] H. Yang and X. S. Liu, "Progress in Paleozoic coal-derived gas exploration in the Ordos Basin, West China," *Petroleum Exploration and Development*, vol. 41, no. 2, pp. 144–152, 2014.

[45] M. Faure, P. Trap, W. Lin, P. Monié, and O. Bruguier, "Polyorogenic evolution of the Paleoproterozoic Trans-North China Belt—new insights from the Lüliangshan-Hengshan-Wutaishan and Fuping massifs," *Episodes*, vol. 30, no. 2, pp. 96–107, 2007.

[46] P. Trap, M. Faure, W. Lin, and S. Meffre, "The Lüliang Massif: a key area for the understanding of the Palaeoproterozoic Trans-North China Belt, North China Craton," *Geological Society - Special Publications*, vol. 323, no. 1, pp. 99–125, 2009.

[47] B. Chuang, C. Yuelong, L. Dapeng, and W. Shanhui, "Provenances of the Mesozoic sediments in the Ordos Basin and implications for collision between the North China Craton (NCC) and the South China Craton (SCC)," *Journal of Asian Earth Sciences*, vol. 96, pp. 296–307, 2014.

[48] H. Woith, R. J. Wang, U. Maiwald, A. Pekdeger, and J. Zschau, "On the origin of geochemical anomalies in groundwaters induced by the Adana 1998 earthquake," *Chemical Geology*, vol. 339, pp. 177–186, 2013.

[49] K. Bräuer, H. Kämpf, S. Niedermann, and G. Strauch, "Monitoring of helium and carbon isotopes in the western Eger Rift area (Czech Republic): relationships with the 2014 seismic activity and indications for recent (2000-2016) magmatic unrest," *Chemical Geology*, vol. 482, pp. 131–145, 2018.

[50] J. du, W. Z. Cheng, Y. L. Zhang et al., "Helium and carbon isotopic compositions of thermal springs in the earthquake zone of Sichuan, Southwestern China," *Journal of Asian Earth Sciences*, vol. 26, no. 5, pp. 533–539, 2006.

[51] X. C. Zhou, L. Liu, Z. Chen, Y. Cui, and J. du, "Gas geochemistry of the hot spring in the Litang fault zone, southeast Tibetan plateau," *Applied Geochemistry*, vol. 79, pp. 17–26, 2017.

[52] R. F. Weiss, "Solubility of helium and neon in water and seawater," *Journal of Chemical & Engineering Data*, vol. 16, no. 2, pp. 235–241, 1971.

[53] J. N. Andrews, "The isotopic composition of radiogenic helium and its use to study groundwater movement in confined aquifers," *Chemical Geology*, vol. 49, no. 1-3, pp. 339–351, 1985.

[54] D. W. Graham, "Noble gas isotope geochemistry of mid-ocean ridge and ocean island basalts: characterization of mantle source reservoirs," *Reviews in Mineralogy and Geochemistry*, vol. 47, pp. 481–538, 2002.

[55] C. J. Ballentine and P. G. Burnard, "Production, release and transport of noble gases in the continental crust," *Reviews in Mineralogy and Geochemistry*, vol. 47, no. 1, pp. 481–538, 2002.

[56] B. A. Mamyrin and I. N. Tolstikhin, *Helium Isotopes in Nature*, Elsevier, 1986.

[57] R. J. Poreda, P. D. Jenden, I. R. Kaplan, and H. Craig, "Mantle helium in Sacramento Basin natural gas wells," *Geochimica et Cosmochimica Acta*, vol. 50, no. 12, pp. 2847–2853, 1986.

[58] J. E. Lupton, "Terrestrial inert gases: isotope tracer studies and clues to primordial components in the mantle," *Annual Review of Earth and Planetary Sciences*, vol. 11, no. 1, pp. 371–414, 1983.

[59] W. M. White, *Isotopic geochemistry*, John Wiley and Sons Ltd, Chichester, 2015.

[60] J. X. Dai, C. N. Zou, S. C. Zhang et al., "Discrimination of abiogenic and biogenic alkane gases," *Science in China Series D: Earth Sciences*, vol. 51, no. 12, pp. 1737–1749, 2008.

[61] S. P. Huang, C. Yu, D. Y. Gong, W. Wu, and F. R. Liao, "Stable carbon isotopic characteristics of alkane gases in tight sandstone gas fields and the gas source in China," *Energy exploration & exploitation*, vol. 32, no. 1, pp. 75–92, 2014.

[62] W. X. Huang, L. H. Yin, and X. Y. Wang, "Assessment of geothermal resources for Qicun geothermal field in Shanxi," *Northwestern Geology*, vol. 36, pp. 87–92, 2003, (in Chinese with English abstract).

[63] G. L. Wang and W. J. Lin, "Main hydro-geothermal systems and their genetic models in China," *Acta Geologica Sinica*, vol. 94, pp. 1923–1937, 2020, (chinese with english abstract).

[64] W. X. Hao, "Geological characteristics and causes of the Houhaoyao geothermal resources in Huailai," *Ground Water*, vol. 37, pp. 29–32, 2015, (in Chinese with English abstract).

[65] X. K. Zhang, C. Y. Wang, G. D. Liu, J. L. Song, and J. C. Wu, "Fine crustal structure in Yanqing-Huailai region by deep seismic reflection profiling," *Acta Geophysica Sinica*, vol. 39, pp. 356–364, 1996, (in Chinese with Enligsh abstract).

[66] Z. X. Huang, H. Y. Li, Y. J. Zheng, and Y. J. Peng, "The lithosphere of North China Craton from surface wave tomography," *Earth and Planetary Science Letters*, vol. 288, no. 1-2, pp. 164–173, 2009.

[67] L. Chen, C. Cheng, and Z. G. Wei, "Seismic evidence for significant lateral variations in lithospheric thickness beneath the central and western North China Craton," *Earth and Planetary Science Letters*, vol. 286, no. 1-2, pp. 171–183, 2009.

[68] J. Zhang, G. C. Zhao, S. Z. Li et al., "Polyphase deformation of the Fuping Complex, Trans-North China Orogen: structures, SHRIMP U-Pb zircon ages and tectonic implications," *Journal of Structural Geology*, vol. 31, no. 2, pp. 177–193, 2009.

[69] W. Lin, Q. C. Wang, J. Wang, F. Wang, Y. Chu, and K. Chen, "Late Mesozoic extensional tectonics of the Liaodong Peninsula massif: response of crust to continental lithosphere destruction of the North China Craton," *Science China Earth Sciences*, vol. 54, no. 6, pp. 843–857, 2011.

[70] L. J. He, "Thermal regime of the North China Craton: implications for craton destruction," *Earth Science Reviews*, vol. 140, pp. 14–26, 2015.

[71] Z. Chen, Y. Li, G. Martinelli, Z. F. Liu, C. Lu, and Y. X. Zhao, "Spatial and temporal variations of CO_2 emissions from the active fault zones in the capital area of China," *Applied Geochemistry*, vol. 112, article 104489, 2020.

[72] J. X. Dai, X. Y. Xia, Y. Z. Wei, and X. Tao, "Carbon isotope characteristics of natural gas in the Sichuan Basin," *Petroleum Geology and Experiment*, vol. 23, pp. 115–121, 2001, (in Chinese with English abstract).

[73] Y. Y. Ni, J. X. Dai, S. Z. Tao et al., "Helium signatures of gases from the Sichuan Basin, China," *Organic Geochemistry*, vol. 74, pp. 33–43, 2014.

[74] L. Chen, W. Tao, L. Zhao, and T. Y. Zheng, "Distinct lateral variation of lithospheric thickness in the northeastern North China Craton," *Earth and Planetary Science Letter*, vol. 267, no. 1-2, pp. 56–68, 2008.

[75] M. K. Li, X. D. Song, J. T. Li, and X. W. Bao, "Lithospheric structures of the main basins in mainland China and its tectonic implications," *Earth Science*, vol. 43, pp. 3362–3372, 2019, (in Chinese with English abstract).

[76] S. B. Hu, L. J. He, and J. Y. Wang, "Heat flow in the continental area of China: a new data set," *Earth and Planetary Science Letters*, vol. 179, no. 2, pp. 407–419, 2000.

[77] A. Minissale, O. Vaselli, D. Chandrasekharam, G. Magro, F. Tassi, and A. Casiglia, "Origin and evolution of 'intracratonic' thermal fluids from central-western peninsular India," *Earth and Planetary Science Letters*, vol. 181, no. 3, pp. 377–394, 2000.

[78] F. Gherardi, C. Panichi, S. Caliro, G. Magro, and M. Pennisi, "Water and gas geochemistry of the Euganean and Berician thermal district (Italy)," *Applied Geochemistry*, vol. 15, no. 4, pp. 455–474, 2000.

[79] R. Kipfer, W. Aeschbach-Hertig, F. Peeters, and M. Stute, "Noble gases in lakes and ground waters," *Reviews in Mineralogy and Geochemistry*, vol. 47, no. 1, pp. 615–700, 2002.

[80] T. P. Fischer, W. F. Giggenbach, Y. Sano, and S. N. Williams, "Fluxes and sources of volatiles discharged from Kudryavy, a subduction zone volcano, Kurile Islands," *Earth and Planetary Science Letters*, vol. 160, no. 1-2, pp. 81–96, 1998.

[81] W. F. Giggenbach, "Variations in the chemical and isotopic composition of fluids discharged from the Taupo Volcanic Zone, New Zealand," *Journal of Volcanology and Geothermal Research*, vol. 68, no. 1-3, pp. 89–116, 1995.

[82] T. H. E. Heaton and J. C. Vogel, ""Excess air" in groundwater," *Journal of Hydrology*, vol. 50, pp. 201–216, 1981.

[83] H. Wycherley, A. Fleet, and H. Shaw, "Some observations on the origins of large volumes of carbon dioxide accumulations in sedimentary basins," *Marine and Petroleum Geology*, vol. 16, no. 6, pp. 489–494, 1999.

[84] G. Chiodini, A. Baldini, F. Barberi et al., "Carbon dioxide degassing at Latera caldera (Italy): evidence of geothermal reservoir and evaluation of its potential energy," *Journal of Geophysical Research*, vol. 112, no. B12, pp. 1–17, 2007.

[85] J. Hoefs, "Some peculiarities in the carbon isotope composition of "juvenile carbon"," *Stable isotopes in the earth sciences*, vol. 200, pp. 181–184, 1978.

[86] M. Javoy, F. Pineau, and C. J. Allègre, "Carbon geodynamic cycle," *Nature*, vol. 300, no. 5888, pp. 171–173, 1982.

[87] K. W. Gould, G. N. Hart, and J. W. Smith, "Technical note: carbon dioxide in the southern coalfields N.S.W.-a factor in the evaluation of natural gas potential," *Proceedings of the Australasian Institute of Mining & Metallurgy*, vol. 279, pp. 41-42, 1981.

[88] R. G. Pankina, V. L. Mekhtiyeva, S. M. Guriyeva, and Y. N. Shkutrik, "Origin of CO_2 in petroleum gases (from the

isotopic composition of carbon)," *International Geology Review*, vol. 21, no. 5, pp. 535–539, 1979.

[89] R. E. Chapman, "Petroleum geochemistry and geology," *Earth Science Reviews*, vol. 16, pp. 60-61, 1980.

[90] J. X. Dai, Y. Song, C. S. Dai, and D. R. Wang, "Geochemistry and accumulation of carbon dioxide gases in China," *AAPG Bulletin*, vol. 80, pp. 1615–1626, 1996.

[91] Y. Sano and B. Marty, "Origin of carbon in fumarolic gas from island arcs," *Chemical Geology*, vol. 119, no. 1-4, pp. 265–274, 1995.

[92] A. Minissale, G. Corti, F. Tassi et al., "Geothermal potential and origin of natural thermal fluids in the northern Lake Abaya area, Main Ethiopian Rift, East Africa," *Journal of Volcanology and Geothermal Research*, vol. 336, pp. 1–18, 2017.

[93] H. Craig, "Isotopic variations in meteoric waters," *Science*, vol. 133, no. 3465, pp. 1702-1703, 1961.

[94] A. Skelton, M. Andrén, H. Kristmannsdóttir et al., "Changes in groundwater chemistry before two consecutive earthquakes in Iceland," *Nature Geoscience*, vol. 7, no. 10, pp. 752–756, 2014.

[95] N. Özgür, E. A. Pala, and S. Degirmenci, "Hydrogeological, hydrogeochemical and isotope geochemical features of the geothermal waters in Seferihisar and Environs, Western Anatolia, Turkey," in *IOP Conference Series: Earth and Environmental Science*, vol. 95, pp. 22–39, Prague, Czech Republic, 2017.

[96] A. Minissale, D. Borrini, G. Montegrossi et al., "The Tianjin geothermal field (north-eastern China): water chemistry and possible reservoir permeability reduction phenomena," *Geothermics*, vol. 37, no. 4, pp. 400–428, 2008.

[97] W. F. Giggenbach, "Isotopic shifts in waters from geothermal and volcanic systems along convergent plate boundaries and their origin," *Earth and planetary science letters*, vol. 113, no. 4, pp. 495–510, 1992.

[98] D. L. Pinti, M. C. Castro, O. Shouakar-Stash et al., "Evolution of the geothermal fluids at Los Azufres, Mexico, as traced by noble gas isotopes, $\delta^{18}O$, δD, $\delta^{13}C$ and $^{87}Sr/^{86}Sr$," *Journal of Volcanology and Geothermal Research*, vol. 249, pp. 1–11, 2013.

[99] H. Chen, "Isotopic fractionation of hydrogen during earth evolution," *China Geology - Journal*, vol. 31, pp. 238–249, 1996, (in Chinese).

[100] D. S. Chapman and H. N. Pollack, "Global heat flow: a new look," *Earth and Planetary Science Letters*, vol. 28, no. 1, pp. 23–32, 1975.

[101] K. P. Furlong and D. S. Chapman, "Crustal heterogeneities and the thermal structure of the continental crust," *Geophysical Research Letters*, vol. 14, no. 3, pp. 314–317, 1987.

[102] J. G. Sclater, C. Jaupart, and D. Galson, "The heat flow through oceanic and continental crust and the heat loss of the earth," *Reviews of Geophysics*, vol. 18, no. 1, pp. 269–311, 1980.

[103] K. W. Nicholson, *Geothermal Fluids: Chemistry and Exploration Techniques*, Springer, Berlin, 2012.

[104] W. F. Giggenbach, "Geothermal solute equilibria. Derivation of Na-K-Mg-Ca geoindicators," *Geochimica et cosmochimica acta*, vol. 52, no. 12, pp. 2749–2765, 1988.

[105] P. Romano and M. Liotta, "Using and abusing Giggenbach ternary Na-K-Mg diagram," *Chemical Geology*, vol. 541, article 119577, 2020.

[106] J. R. Liu, X. F. Song, G. F. Yuan, X. M. Sun, X. Liu, and S. Q. Wang, "Characteristics of $\delta^{18}O$ in precipitation over Eastern Monsoon China and the water vapor sources," *Chinese Science Bulletin*, vol. 55, no. 2, pp. 200–211, 2010.

[107] V. M. Merwade, D. R. Maidment, and J. A. Goff, "Anisotropic considerations while interpolating river channel bathymetry," *Journal of Hydrology*, vol. 331, no. 3-4, pp. 731–741, 2006.

[108] F. Huang, L. J. He, and Q. J. Wu, "Lithosperic thermal structure of the Ordos Basin and its implications to destruction of the North China Craton," *Chinese Journal of Geophysics*, vol. 58, pp. 3671–3686, 2015, (in Chinese with English abstract).